COMPUTER METHODS IN APPLIED MECHANICS AND ENGINEERING 73 (1989) 53–92
NORTH-HOLLAND

ON A STRESS RESULTANT GEOMETRICALLY EXACT SHELL MODEL. PART II: THE LINEAR THEORY; COMPUTATIONAL ASPECTS

J.C. SIMO, D.D. FOX and M.S. RIFAI
Division of Applied Mechanics, Department of Mechanical Engineering, Stanford University, Stanford, CA, U.S.A.

Received 2 October 1987
Revised manuscript received 7 June 1988

Computational aspects of a linear stress resultant (classical) shell theory, obtained by systematic linearization of the geometrically exact nonlinear theory, considered in Part I of this work, are examined in detail. In particular, finite element interpolations for the reference director field and the linearized rotation field are constructed such that the underlying geometric structure of the continuum theory is preserved exactly by the discrete approximation. A discrete canonical, *singularity-free* mapping between the five and the six degree of freedom formulation is constructed by exploiting the geometric connection between the orthogonal group (SO(3)) and the unit sphere (S^2). The proposed numerical treatment of the membrane and bending fields, based on a mixed Hellinger–Reissner formulation, provides excellent results for the 4-node bilinear isoparametric element. As an example, convergent results are obtained for rather *coarse* meshes in fairly demanding, singularity-dominated, problems such as the classical rhombic plate test. The proposed theory and finite element implementation are evaluated through an extensive set of benchmark problems. The results obtained with the present approach exactly match previous solutions obtained with state-of-the-art implementations based on the so-called *degenerated solid approach*.

1. Introduction

In this paper, we address in detail numerical aspects involved in the finite element implementation of a *classical linear stress-resultant* shell theory. The proposed formulation is obtained by a systematic linearization about the refence state of the geometrically exact fully nonlinear theory developed in Part I of this work [32].[1] The resulting theory is termed "classical" in the following sense:

(i) The momentum equations, formulated directly in terms of resultants, are *exact* within the framework of a directed media or Cosserat continuum. These equations involve stress resultants whose definitions agree with those of classical shell theory, but are at variance with definitions often employed in the degenerated solid approach which dominates the current computational literature. An example of this variance is the definition of the membrane stress resultants. It is a well-known classical result, see [25, 26], that these stress resultants *can never be symmetric* due to the initial curvature of the shell. It is also a classical result, which carries

[1]The term "geometrically exact" reflects the fact that no additional kinematic assumptions are made beyond the one-director assumption. In particular, approximations of the type $\sin\Theta \simeq \Theta - \Theta^3/6$ are entirely avoided.

over to shell models allowing for shear deformation, that only a certain combination of the resultant membrane stresses and the resultant bending stress couples, known as the *effective stress resultants* appears in the internal stress power. Remarkably, this is the only relevant object in a weak formulation of the field equations.

(ii) The constitutive equations are formulated directly in terms of resultant stress and stress couples. Classically, the constitutive coefficients entering in these equations can be determined a priori by several standard procedures; i.e., asymptotic expansion of the three-dimensional theory, or invariance arguments along with matching of exact simple three-dimensional solutions. An important fact, demonstrated numerically in the following sections, is that these simple constitutive models, which do not involve the costly pre-integration through the thickness (a main feature of the degenerated solid approach), reproduce the exact solutions of standard benchmark problems. We also note that three-dimensional constitutive models can be pre-integrated numerically, if so desired, to obtain stress resultant models that fit within the classical approach.

(iii) An important difference between the present formulation and classical shell theories, however, concerns the parametrization and format in which the field equations are cast. From the summary of the linear theory in Table 1, it is apparent that objects such as Christoffel symbols, the second fundamental form, and covariant derivatives, *which are not readily accessible* in a computational framework, *never appear explicitly*. A further difference concerns the central role played by the underlying geometric structure of the theory. As an example, by exploiting the relation between the orthogonal group and the unit sphere, we construct a unique orthogonal transformation that maps the inertial frame onto an orthonormal director frame without "drill" about the director.

The objective of this paper is to demonstrate that classical shell theory, rephrased in the format of Table 1, is amenable to a straightforward finite element implementation. In particular, because of our parametrization of the field equations, the implementation is closely related to numerical treatments of the classical Reissner–Mindlin plate model. From a computational standpoint, novel aspects present in our approach are the following:

(iv) Construction of the interpolations for the reference director and the linearized director field that exactly preserve the kinematic structure of the theory; i.e., the discretized reference director has unit length, and the incremental rotation field is orthogonal to the director throughout the element.

(v) Transformation from six to five degrees of freedom formulation by means of a *unique orthogonal transformation* that maps the inertial frame onto an *orthonormal* director frame *without drill*. (Geometrically this is accomplished by reducing SO(3) by S^1.)

Our numerical implementation is carried out with reference to the four-node bilinear isoparametric element. Within the context of linear Mindlin–Reissner plate theory, several interpolation schemes have been proposed to ameliorate the well-known *shear locking effect* which typically arises as the thickness of the plate goes to zero. In the present context, we accommodate a scheme that essentially goes back to MacNeal [20], subsequently extended and reformulated in Hughes and Tezduyar [16], and MacNeal [21], and revisited in Bathe and Dvorkin [5]. The only available mathematical analysis of this scheme, to some extent incomplete, is due to Bathe and Brezzi [34]. To our knowledge, a complete mathematical analysis comparable to the recent work of Brezzi and Fortin [9] and Arnold and Falk [1] for a triangular element, for which these authors prove rigorous *uniform convergence estimates* for

Table 1
The linear theory. Summary

- Resultant stress couple vectors:

$$\tilde{n} = \begin{Bmatrix} \tilde{n}^{11} \\ \tilde{n}^{22} \\ \tilde{n}^{12} \end{Bmatrix}, \qquad \tilde{q} = \begin{Bmatrix} \tilde{q}^{1} \\ \tilde{q}^{2} \end{Bmatrix}, \qquad \tilde{m} = \begin{Bmatrix} \tilde{m}^{11} \\ \tilde{m}^{22} \\ \tilde{m}^{12} \end{Bmatrix}$$

- Orthogonal transformation: [such that $\Lambda^0(E \times t^0) = (E \times t^0)$]

$$t_\alpha^0 = \Lambda^0 E \quad \text{and} \quad t^0 = \Lambda^0 E$$

$$\Lambda^0 = [t_1\ t_2\ t] = (E \cdot t^0)1_3 + [\widehat{E \times t^0}] + \frac{1}{1 + E \cdot t^0}(E \times t^0) \otimes (E \times t^0)$$

- Incremental displacement and rotation: $[\Delta t \cdot t^0 = \Delta T \cdot E = 0]$

$$u = \begin{Bmatrix} u^1 \\ u^2 \\ u^3 \end{Bmatrix}, \qquad \Delta t = \bar{\Lambda}^0 \Delta T, \qquad \Delta T = \begin{Bmatrix} \Delta T^1 \\ \Delta T^2 \end{Bmatrix} \quad \text{and} \quad \bar{\Lambda}^0 := [t_1\ t_2] = \begin{bmatrix} \Lambda_{11}^0 & \Lambda_{12}^0 \\ \Lambda_{21}^0 & \Lambda_{22}^0 \\ \Lambda_{31}^0 & \Lambda_{32}^0 \end{bmatrix}$$

- Matrix differential operators:

$$\mathbb{B}_m = \begin{bmatrix} \varphi_{,1}^{0t} \dfrac{\partial}{\partial \xi^1} \\ \varphi_{,2}^{0t} \dfrac{\partial}{\partial \xi^2} \\ \varphi_{,1}^{0t} \dfrac{\partial}{\partial \xi^2} + \varphi_{,2}^{0t} \dfrac{\partial}{\partial \xi^1} \end{bmatrix}_{3\times 3}$$

$$\mathbb{B}_{sm} = \begin{bmatrix} t^{0t} \dfrac{\partial}{\partial \xi^1} \\ t^{0t} \dfrac{\partial}{\partial \xi^2} \end{bmatrix}_{2\times 3} \qquad \mathbb{B}_{sb} = \begin{bmatrix} \varphi_{,1}^{0t} \\ \varphi_{,2}^{0t} \end{bmatrix}_{2\times 3} \bar{\Lambda}^0_{3\times 2}$$

$$\mathbb{B}_{bm} = \begin{bmatrix} t_{,1}^{0t} \dfrac{\partial}{\partial \xi^1} \\ t_{,2}^{0t} \dfrac{\partial}{\partial \xi^2} \\ t_{,1}^{0t} \dfrac{\partial}{\partial \xi^2} + t_{,2}^{0t} \dfrac{\partial}{\partial \xi^1} \end{bmatrix}_{3\times 3} \qquad \mathbb{B}_{bb} = \begin{bmatrix} \varphi_{,1}^{0t} \dfrac{\partial}{\partial \xi^1} \\ \varphi_{,2}^{0t} \dfrac{\partial}{\partial \xi^2} \\ \varphi_{,1}^{0t} \dfrac{\partial}{\partial \xi^2} + \varphi_{,2}^{0t} \dfrac{\partial}{\partial \xi^1} \end{bmatrix} \bar{\Lambda}^0_{3\times 2}$$

- Bilinear form B: $T_{\Phi^0}\mathscr{C} \times T_{\Phi^0}\mathscr{C} \to \mathbb{R}$:

$$B = \int_{\mathscr{A}} \{[\mathbb{B}_m v]^t \tilde{n} + [\mathbb{B}_{sm} v + \mathbb{B}_{sb}\, \delta T]^t \tilde{q} + [\mathbb{B}_{bm} v + \mathbb{B}_{bb}\, T]^t \tilde{m}\}\, d\mu^0$$

any thickness, is still lacking. The emphasis in this work, however, is not placed on the development of (yet) another shell element, but rather on the implementation and numerical assessment of a mechanically sound methodology that finds its roots in classical shell theory. Nevertheless, some interesting conclusions from the purely computational standpoint emanate from the present work. In particular:

(vi) The proposed mixed interpolation for the bending field, which emanates from a Hellinger–Reissner variational formulation, leads to an element which possesses proper rank, and yields excellent results in standard benchmark problems. For the classical rhombic plate test (a singularity-dominated problem) for instance, the performance of the element is clearly superior to existing four-node and even nine-node elements; including T1 [16], the equivalent element of Bathe and Dvorkin [5], and the four- and nine-node ANS formulations of Stanley [38] and Parks and Stanley [27].

(vii) The interpolation for the membrane field, inspired in the treatment of Pian and Sumihara [29] for the plane stress problem, also appears to yield optimal results (for bilinear interpolations) in numerical experiments involving membrane dominated problems; such as *Cook's membrane test*, and the Scordellis–Lo [31] test.

Although the finite element interpolation satisfies exactly all patch test requirments, (this is at variance with some recently proposed *assumed strain interpolations* [18][2]) a satisfactory mathematical analysis is still lacking.

2. Summary of the governing equations

In this section, we summarize the basic field equations governing the proposed linear shell model. These equations emanate from the nonlinear theory examined in detail in Part I of the work. We begin with a review of the nonlinear theory.

2.1. *The nonlinear theory. Summary*

We limit our presentation on the nonlinear theory to a brief overview of the basic kinematics, field equations, weak form of the balance equations, and constitutive equations. For further details, we refer to [32, 33].

2.1.1. *The basic kinematics*

Let $S^2 := \{t \in \mathbb{R}^3 \mid \|t\| = 1\}$ be the unit sphere and $T_t S^2 := \{\omega \in \mathbb{R}^3 \mid t \cdot \omega = 0\}$ be the tangent space at $t \in S^2$. The configuration space of the shell, denoted by $\mathscr{C}$, is defined

$$\mathscr{C} := \{\Phi := (\varphi, t) : \bar{\mathscr{A}} \subset \mathbb{R}^2 \to \mathbb{R}^3 \times S^2\} . \tag{2.1}$$

Here, $\bar{\mathscr{A}} \subset \mathbb{R}^2$ is compact, with boundary $\partial\mathscr{A}$. We denote by $\partial_\varphi \mathscr{A} \subset \partial\mathscr{A}$ and $\partial_t \mathscr{A} \subset \partial\mathscr{A}$ the regions of $\partial\mathscr{A}$ with prescribed displacements and rotations, respectively.

The basic kinematic assumption can be formulated as follows. Let $\mathscr{S}$ denote *any* configuration of the shell. It is assumed that

$$\mathscr{S} := \{x \in \mathbb{R}^3 \mid x = \varphi + \xi t \text{ where } (\varphi, t) \in \mathscr{C} \text{ and } \xi \in [h^-, h^+]\} , \tag{2.2}$$

where $h = h^+ - h^-$ is the thickness of the shell, $\varphi : \bar{\mathscr{A}} \subset \mathbb{R}^2 \to \mathbb{R}^3$ defines the mid-surface of the shell, and $t(\xi^1, \xi^2) \in S^2$, for $(\xi^1, \xi^2) \in \bar{\mathscr{A}}$.

[2] Our numerical experiments appear to indicate that this nine-node element does not pass constant membrane and bending patch tests.

2.1.2. Momentum balance equations

The (exact) local momentum equations are expressed in stress resultants and stress couples as

$$\frac{1}{\bar{j}}(\bar{j}\boldsymbol{n}^{\alpha})_{,\alpha} + \bar{\boldsymbol{n}} = \bar{\rho}\ddot{\boldsymbol{\varphi}}\,, \qquad \frac{1}{\bar{j}}(\bar{j}\tilde{\boldsymbol{m}}^{\alpha})_{,\alpha} - \bar{\boldsymbol{l}} + \tilde{\bar{\boldsymbol{m}}} = \bar{I}_{\rho}\ddot{\boldsymbol{t}}\,, \tag{2.3}$$

where $\boldsymbol{n}^{\alpha} = n^{\beta\alpha}\boldsymbol{\varphi}_{,\beta} + q^{\alpha}\boldsymbol{t}$ and $\tilde{\boldsymbol{m}}^{\alpha} = \tilde{m}^{\beta\alpha}\boldsymbol{\varphi}_{,\beta} + \tilde{m}^{3\alpha}\boldsymbol{t}$ are the resultant stress and the director couple resultants, $\bar{\boldsymbol{n}}$ and $\tilde{\bar{\boldsymbol{m}}}$ are the applied loads, $\bar{j} = \|\boldsymbol{\varphi}_{,1} \times \boldsymbol{\varphi}_{,2}\|$ is the surface Jacobian, and $\bar{\boldsymbol{l}} = \lambda\boldsymbol{t} + \boldsymbol{l}$, where $\boldsymbol{l}$ is the across-the-thickness stress resultant.

In addition to balance equations (2.3), there is a further constraint that balance of angular momentum places on the admissible form of the constitutive equations. This constitutive restriction (emanating from the symmetry condition $\boldsymbol{\sigma} = \boldsymbol{\sigma}^{t}$) is given by

$$\boldsymbol{\varphi}_{,\alpha} \times \boldsymbol{n}^{\alpha} + \boldsymbol{t}_{,\alpha} \times \tilde{\boldsymbol{m}}^{\alpha} + \boldsymbol{t} \times \boldsymbol{l} = \boldsymbol{0}\,. \tag{2.4}$$

By systematically exploiting this restriction (see Part I of this work for details), we obtain *effective membrane* and *effective shear resultant* forces, denoted by $\tilde{\boldsymbol{n}} = \tilde{n}^{\alpha\beta}\boldsymbol{\varphi}_{,\alpha} \otimes \boldsymbol{\varphi}_{,\beta}$ and $\tilde{\boldsymbol{q}} = \tilde{q}^{\alpha}\boldsymbol{\varphi}_{,\alpha}$, respectively, and defined by the relations

$$\begin{aligned} \tilde{n}^{\beta\alpha} &:= n^{\beta\alpha} - \lambda^{\beta}_{\mu}\tilde{m}^{\alpha\mu} \equiv \tilde{n}^{\alpha\beta}\,, \\ \tilde{q}^{\alpha} &:= q^{\alpha} - \lambda^{3}_{\mu}\tilde{m}^{\alpha\mu}\,, \\ \boldsymbol{l} &= \lambda\boldsymbol{t} + (\tilde{q}^{\alpha} + \lambda^{\alpha}_{\mu}\tilde{m}^{3\mu})\boldsymbol{\varphi}_{,\alpha}\,, \end{aligned} \tag{2.5}$$

where $\boldsymbol{t}_{,\alpha} = \lambda^{\beta}_{\alpha}\boldsymbol{\varphi}_{,\beta} + \lambda^{3}_{\alpha}\boldsymbol{t}$. Note that $\tilde{\boldsymbol{n}} = \tilde{\boldsymbol{n}}^{t}$, but $n^{\alpha\beta} \neq n^{\beta\alpha}$.

2.1.3. Weak form of the momentum balance equations

Recall that the tangent space of kinematically admissible variations is given by

$$\mathrm{T}_{\boldsymbol{\Phi}}\mathscr{C} = \{(\delta\boldsymbol{\varphi}, \delta\boldsymbol{t}) =: \delta\boldsymbol{\Phi} : \bar{\mathscr{A}} \to \mathbb{R}^3 \times \mathrm{T}_{t}\mathrm{S}^2 \,|\, \delta\boldsymbol{\varphi}|_{\partial_{\boldsymbol{\varphi}}\mathscr{A}} = \boldsymbol{0} \text{ and } \delta\boldsymbol{t}|_{\partial_{t}\mathscr{A}} = \boldsymbol{0}\}\,, \tag{2.6}$$

where the condition $\delta\boldsymbol{t} \in \mathrm{T}_{t}\mathrm{S}^2$ implies $\boldsymbol{t} \cdot \delta\boldsymbol{t} = 0$.

By taking the dot product of the momentum equations with an arbitrary variation $\delta\boldsymbol{\Phi} \in \mathrm{T}_{\boldsymbol{\Phi}}\mathscr{C}$ and integrating by parts, one obtains the weak form of the momentum balance equations as

$$G_{\mathrm{dyn}}(\boldsymbol{\Phi}, \delta\boldsymbol{\Phi}) := G(\boldsymbol{\Phi}, \delta\boldsymbol{\Phi}) + \int_{\bar{\mathscr{A}}} [\bar{\rho}\ddot{\boldsymbol{\varphi}} \cdot \delta\boldsymbol{\varphi} + \bar{I}_{\rho}\ddot{\boldsymbol{t}} \cdot \delta\boldsymbol{t}]\, \mathrm{d}\mu\,. \tag{2.7}$$

Here, $\mathrm{d}\mu = \bar{j}\,\mathrm{d}\xi^1\,\mathrm{d}\xi^2$ is the current surface measure and $G(\boldsymbol{\Phi}, \delta\boldsymbol{\Phi})$ is the static weak form defined as

$$G(\boldsymbol{\Phi}, \delta\boldsymbol{\Phi}) := \int_{\mathscr{A}} [\boldsymbol{n}^{\alpha} \cdot \delta\boldsymbol{\varphi}_{,\alpha} + \tilde{\boldsymbol{m}}^{\alpha} \cdot \delta\boldsymbol{t}_{,\alpha} + \boldsymbol{l} \cdot \delta\boldsymbol{t}]\, \mathrm{d}\mu - G_{\mathrm{ext}}(\delta\boldsymbol{\Phi})\,, \tag{2.8}$$

where $G_{ext}(\delta\Phi)$: $T_{\Phi}\mathscr{C} \to \mathbb{R}$ is the virtual work of the external loading given by

$$G_{ext}(\delta\Phi) = \int_{\mathscr{A}} [\bar{n}\cdot\delta\varphi + \tilde{\bar{m}}\cdot\delta t]\,d\mu + \int_{\partial_n\mathscr{A}} \bar{\bar{n}}\cdot\delta\varphi\bar{j}\,ds + \int_{\partial_m\mathscr{A}} \bar{\bar{m}}\cdot\delta t\bar{j}\,ds\,. \tag{2.9}$$

In this expression, $\bar{\bar{n}}$ and $\bar{\bar{m}}$ are the prescribed resultant force and the prescribed director couple on the boundary $\partial_n\mathscr{A}$ and $\partial_m\mathscr{A}$, respectively, where

$$\partial_n\mathscr{A} \cap \partial_\varphi\mathscr{A} = \emptyset \quad \text{and} \quad \partial_m\mathscr{A} \cap \partial_t\mathscr{A} = \emptyset\,. \tag{2.10}$$

Introducing the strain measures[3]

$$\varepsilon_{\alpha\beta} := \tfrac{1}{2}(\varphi_{,\alpha}\cdot\varphi_{,\beta} - \varphi^0_{,\alpha}\cdot\varphi^0_{,\beta})\,, \tag{2.11a}$$

$$\gamma_\alpha := (\varphi_{,\alpha}\cdot t - \varphi^0_{,\alpha}\cdot t^0)\,, \tag{2.11b}$$

$$\rho_{\alpha\beta} := (\varphi_{,\alpha}\cdot t_{,\beta} - \varphi^0_{,\alpha}\cdot t^0_{,\beta})\,, \tag{2.11c}$$

it can be shown that *only the symmetric* effective membrane stress resultant appears in the static weak form (2.8) which now takes the form

$$G(\Phi, \delta\Phi) = \int_{\mathscr{A}} [\tilde{n}^{\alpha\beta}\delta\varepsilon_{\alpha\beta} + \tilde{m}^{\alpha\beta}\delta\rho_{\alpha\beta} + \tilde{q}^\alpha\delta\gamma_\alpha]\,d\mu - G_{ext}(\delta\Phi)\,. \tag{2.12}$$

Note that the components in expression (2.12) of the static weak form are given relative to the surface convected (Gaussian) frame $\{\varphi_{,1}, \varphi_{,2}, t\}$. An alternative expression involving components relative to a local cartesian system is considered in Section 3.

2.1.4. Constitutive equations

The simplest example of a properly invariant elastic isotropic constitutive model for the stress resultants in terms of the conjugate strain measures (2.11) is given by

$$\begin{aligned} \tilde{n}^{\alpha\beta} &= \frac{Eh}{1-\nu^2}\,H_0^{\alpha\beta\gamma\delta}\varepsilon_{\gamma\delta}\,, \qquad \tilde{q}^\alpha = \kappa G^s h a^{0\alpha\beta}\gamma_\beta\,, \\ \tilde{m}^{(\alpha\beta)} &= \frac{Eh^3}{12(1-\nu^2)}\,H_0^{\alpha\beta\gamma\delta}\rho_{(\gamma\delta)}\,, \end{aligned} \tag{2.13}$$

where E is Young's modulus, ν is Poisson's ratio, κ is the shear reduction coefficient, G^s is the shear modulus, $a^0_{\alpha\beta} := \varphi^0_{,\alpha}\cdot\varphi^0_{,\beta}$ is the reference surface metric, and

$$H_0^{\alpha\beta\gamma\delta} = \{\nu a^{0\alpha\beta}a^{0\gamma\delta} + \tfrac{1}{2}(1-\nu)(a^{0\alpha\gamma}a^{0\beta\delta} + a^{0\alpha\delta}a^{0\beta\gamma})\}\,. \tag{2.14}$$

REMARK 2.1. The constitutive equations for the resultant director couple is given in terms of the symmetric part of $\tilde{m}^{\alpha\beta}$. Without loss of generality, it is assumed here and in the following developments that the skew-symmetric part of $\tilde{m}^{\alpha\beta}$ is zero, i.e.

[3] In Part I, the shear strain (2.11b) was denoted δ_α.

$$\tilde{m}^{[\alpha\beta]} = 0 . \tag{2.15}$$

Asymptotic expansions of the three-dimensional theory reveal that $\tilde{m}^{[\alpha\beta]} = O(h^3/RL^2)$, where h is the thickness, R is the radius of curvature of the shell, and L is a suitable in-plane length scale of order O(1). Hence, the skew-symmetric part $\tilde{m}^{[\alpha\beta]}$ can be neglected within the order of approximation of the linear theory. □

2.2. *Linearization. The model problem*

We now proceed to linearize the nonlinear theory about the reference state $(\varphi^0, t^0) \in \mathscr{C}$. To this end, let $(u, \Delta t)$: $\bar{\mathscr{A}} \to \mathbb{R}^3 \times T_{t^0}S^2$ be the displacement field for the reference state. Making use of the exponential map in S^2, consider the curve $\varepsilon \mapsto (\varphi^0_\varepsilon, t^0_\varepsilon) \in \mathscr{C}$ defined as

$$\begin{aligned} &\varepsilon \mapsto \varphi^0_\varepsilon = \varphi^0 + \varepsilon u , \\ &\varepsilon \mapsto t^0_\varepsilon = \cos|\varepsilon\,\Delta t| t^0 + \frac{\sin|\varepsilon\,\Delta t|}{|\varepsilon\,\Delta t|}\,\varepsilon\,\Delta t = t^0 + \varepsilon\,\Delta t + O(\varepsilon^2) . \end{aligned} \tag{2.16}$$

From the discussion in Part I of this work, we recall that $\Delta t \in T_{t^0}S^2$, i.e. $t^0 \cdot \Delta t = 0$, and that there exists a unique Λ^0, satisfying $\Lambda^{0-1} = [\Lambda^0]^t$ and $\Lambda^0 \psi = \psi$ with $\psi \cdot E = 0$, such that $t^0 = \Lambda^0 E$. We thus define $\Delta t \in T_{t^0}S^2$ by the relation $\Delta t = \Lambda^0 \Delta T$, where $\Delta T \cdot E = 0$.

If one selects $E \equiv E_3$, then ΔT is given in components relative to the standard basis as

$$\Delta T = \Delta T^1 E_1 + \Delta T^2 E_2 . \tag{2.17}$$

Therefore, by expressing the incremental *spatial* rotation vector as $\Delta t = \Lambda^0 \Delta T$, where ΔT is given by (2.17), the constraint condition $\Delta t \cdot t^0 = 0$ is identically satisfied since $\Delta T \cdot E = \Delta t \cdot t^0 = 0$. This observation is crucial to the numerical implementation considered below.

Use of construction (2.16) yields the following expression for the strain measures defined by (2.11):

$$\begin{aligned} \varepsilon_{\alpha\beta} &:= \tfrac{1}{2}\varepsilon(\varphi^0_{,\alpha} \cdot u_{,\beta} + u_{,\alpha} \cdot \varphi^0_{,\beta}) + O(\varepsilon^2) , \\ \gamma_\alpha &:= \varepsilon(\varphi^0_{,\alpha} \cdot \Delta t + u_{,\alpha} \cdot t^0) + O(\varepsilon^2) , \\ \rho_{\alpha\beta} &:= \varepsilon(\varphi^0_{,\alpha} \cdot \Delta t_{,\beta} + u_{,\alpha} \cdot t^0_{,\beta}) + O(\varepsilon^2) . \end{aligned} \tag{2.18}$$

By making use of the directional derivative formula and setting $\delta(\bullet) = (d/d\varepsilon)|_{\varepsilon=0}(\bullet)$, we obtain the linearized strain measures about the reference state as

$$\begin{aligned} \delta\varepsilon_{\alpha\beta} &:= \bar{\varepsilon}_{\alpha\beta} = \tfrac{1}{2}(\varphi^0_{,\alpha} \cdot u_{,\beta} + u_{,\alpha} \cdot \varphi^0_{,\beta}) , \\ \delta\gamma_\alpha &:= \bar{\gamma}_\alpha = (\varphi^0_{,\alpha} \cdot \Delta t + u_{,\alpha} \cdot t^0) , \\ \delta\rho_{(\alpha\beta)} &:= \bar{\rho}_{(\alpha\beta)} = \tfrac{1}{2}(\varphi^0_{,\alpha} \cdot \Delta t_{,\beta} + \varphi^0_{,\beta} \cdot \Delta t_{,\alpha} + u_{,\alpha} \cdot t^0_{,\beta} + u_{,\beta} \cdot t^0_{,\alpha}) , \end{aligned} \tag{2.19}$$

where only the symmetric part of $\rho_{\alpha\beta}$ is considered.

Table 2
Example: Elastic isotropic constitutive equations

Lowest-order constitutive model

- Reference surface metric:

$$a^0_{\alpha\beta} = \boldsymbol{\varphi}^0_{,\alpha} \cdot \boldsymbol{\varphi}^0_{,\beta}$$

- Elastic isotropic constitutive equations:

$$\boldsymbol{H} = \begin{bmatrix} a^{0\,11}a^{0\,11} & \left(\begin{matrix}\nu a^{0\,11}a^{0\,22}+\\(1-\nu)a^{0\,12}a^{0\,12}\end{matrix}\right) & a^{0\,11}a^{0\,12} \\ \left(\begin{matrix}\nu a^{0\,11}a^{0\,22}+\\(1-\nu)a^{0\,12}a^{0\,12}\end{matrix}\right) & a^{0\,22}a^{0\,22} & a^{0\,22}a^{0\,12} \\ a^{0\,11}a^{0\,12} & a^{0\,22}a^{0\,12} & \left(\begin{matrix}\frac{1-\nu}{2}\,a^{0\,11}a^{0\,22}+\\\frac{(1+\nu)}{2}\,a^{0\,12}a^{0\,12}\end{matrix}\right) \end{bmatrix}$$

$$\begin{Bmatrix}\tilde{n}^{11}\\ \tilde{n}^{22}\\ \tilde{n}^{12}\end{Bmatrix} = \frac{Eh}{1-\nu^2}\,\boldsymbol{H}\begin{Bmatrix}\bar{\varepsilon}_{11}\\ \bar{\varepsilon}_{22}\\ 2\bar{\varepsilon}_{12}\end{Bmatrix}, \qquad \begin{Bmatrix}\tilde{q}^1\\ \tilde{q}^2\end{Bmatrix} = \kappa Gh\begin{bmatrix}a^{0\,11} & a^{0\,12}\\ a^{0\,12} & a^{0\,22}\end{bmatrix}\begin{Bmatrix}\bar{\gamma}_1\\ \bar{\gamma}_2\end{Bmatrix},$$

$$\begin{Bmatrix}\tilde{m}^{11}\\ \tilde{m}^{22}\\ \tilde{m}^{12}\end{Bmatrix} = \frac{Eh^3}{1-\nu^2}\,\boldsymbol{H}\begin{Bmatrix}\bar{\rho}_{11}\\ \bar{\rho}_{22}\\ 2\bar{\rho}_{(12)}\end{Bmatrix}$$

Higher-order constitutive model

- Second fundamental form:

$$b^0_{\alpha\beta} = \boldsymbol{n}^0_{,\alpha} \cdot \boldsymbol{\varphi}^0_{,\beta}, \quad \text{where } \boldsymbol{n}^0 \cdot \boldsymbol{\varphi}^0_{,\alpha} = 0$$

$$d^0_{\alpha\beta} = \boldsymbol{n}^0_{,\alpha} \cdot \boldsymbol{n}^0_{,\beta}$$

- Constitutive tensors:

$$H_0^{\alpha\beta\gamma\delta} = \left\{\nu a^{0\alpha\beta}a^{0\gamma\delta} + \frac{(1-\nu)}{2}\,(a^{0\alpha\gamma}a^{0\beta\delta} + a^{0\alpha\delta}a^{0\beta\gamma})\right\},$$

$$H_1^{\alpha\beta\gamma\delta} = \left\{\nu(a^{0\alpha\beta}b^{0\gamma\delta} + a^{0\gamma\delta}b^{0\alpha\beta}) + \frac{(1-\nu)}{2}\,(a^{0\alpha\gamma}b^{0\beta\delta} + a^{0\beta\delta}b^{0\alpha\gamma} + a^{0\alpha\delta}b^{0\beta\gamma} + a^{0\beta\gamma}b^{0\alpha\delta})\right\},$$

$$H_2^{\alpha\beta\gamma\delta} = \left\{\nu b^{0\alpha\beta}b^{0\gamma\delta} + \frac{(1-\nu)}{2}\,(b^{0\alpha\gamma}b^{0\beta\delta} + b^{0\alpha\delta}b^{0\beta\gamma})\right\}$$

$$H_3^{\alpha\beta\gamma\delta} = \left\{\nu(a^{0\alpha\beta}d^{0\gamma\delta} + a^{0\gamma\delta}d^{0\alpha\beta}) + \frac{(1-\nu)}{2}\,(a^{0\alpha\gamma}d^{0\beta\delta} + a^{0\beta\delta}d^{0\alpha\gamma} + a^{0\alpha\delta}d^{0\beta\gamma} + a^{0\beta\gamma}d^{0\alpha\delta})\right\}$$

- Membrane and bending stress resultants:

$$\tilde{n}^{\alpha\beta} = \frac{E}{1-\nu^2}\left(hH_0^{\alpha\beta\gamma\delta}\bar{\varepsilon}_{\gamma\delta} - \frac{h^3}{6}\,H_1^{\alpha\beta\gamma\delta}\bar{\rho}_{(\gamma\delta)} + \frac{h^3}{3}\,H_2^{\alpha\beta\gamma\delta}\bar{\varepsilon}_{\gamma\delta} + \frac{h^3}{4}\,H_3^{\alpha\beta\gamma\delta}\bar{\varepsilon}_{\gamma\delta}\right),$$

$$\tilde{m}^{(\alpha\beta)} = \frac{E}{1-\nu^2}\left(\frac{h^3}{12}\,H_0^{\alpha\beta\gamma\delta}\bar{\rho}_{(\gamma\delta)} - \frac{h^3}{6}\,H_1^{\alpha\beta\gamma\delta}\bar{\varepsilon}_{\gamma\delta}\right)$$

$$\tilde{q}^\alpha = \kappa G\left(ha^{0\alpha\beta} + \frac{h^3}{4}\,d^{0\alpha\beta}\right)\gamma_\beta$$

REMARKS 2.2. (1) In classical developments of linear shell theory, the bending strain measure $\bar{\rho}_{(\alpha\beta)}$ is often replaced by $\bar{\rho}_{(\alpha\beta)}$ plus a linear combination involving products of $\bar{\varepsilon}_{\alpha\beta}$ and the second fundamental form of the surface $b^0_{\alpha\beta} := \boldsymbol{n}^0_{,\alpha} \cdot \boldsymbol{\varphi}^0_{,\alpha}$. This is the case in the "best linear theory" of Budiansky and Sanders [10], where the bending strain measure $\tilde{\rho}_{\alpha\beta} := \bar{\rho}_{(\alpha\beta)} - \frac{1}{2}[b^{0\gamma}_{\alpha}\bar{\varepsilon}_{\gamma\beta} + b^{0\gamma}_{\beta}\bar{\varepsilon}_{\gamma\alpha}]$, first proposed by Sanders [30], is employed. The two motivations for this choice are: (a) the resulting theory reduces to Love's first approximation for spherical geometry, and (b) $\tilde{\rho}_{\alpha\beta}$ vanishes identically for constant displacement fields normal to the mid-surface. Our numerical experiments indicate that no significant difference is obtained using either strain measure.

(2) Strictly speaking, changing the strain measure while holding fixed the structure of the constitutive equation, yields a different constitutive model. However, as noted by several authors, see e.g., Naghdi [25, p. 606], or Niordson [26], the constitutive models differ in terms involving products of the first and second fundamental form, which can be argued to be of higher order. In this regard, our numerical experiments yield indistinguishable results for both constitutive models in Table 2. These two models differ only in terms involving products of the first and second fundamental forms.

(3) The remark above suggests that numerical integration through the thickness of simple three-dimensional elastic constitutive equations, a standard paractice in the degenerated solid approach, is a costly procedure which leads to no improved accuracy for most thin, or moderately thick, shell problems. □

2.3. *Linearized static weak form. Matrix expressions*

The static weak form of the momentum equations, linearized about the reference state, is obtained in the standard manner by means of the Gateaux (directional) derivative formula. This leads to the bilinear form B: $\mathrm{T}_{\boldsymbol{\Phi}^0}\mathscr{C} \times \mathrm{T}_{\boldsymbol{\Phi}^0}\mathscr{C} \to \mathbb{R}$ defined as

$$B \equiv \mathrm{D}G(\boldsymbol{\Phi}^0; (\boldsymbol{v}, \delta t)) \cdot (\boldsymbol{u}, \Delta t) := \frac{\mathrm{d}}{\mathrm{d}\varepsilon}\bigg|_{\varepsilon=0} G(\boldsymbol{\Phi}^0_\varepsilon; (\boldsymbol{v}, \delta t)), \tag{2.20}$$

where $\boldsymbol{\Phi}^0_\varepsilon = (\boldsymbol{\varphi}^0_\varepsilon, t^0_\varepsilon)$ is constructed as in (2.16) with variations $(\boldsymbol{u}, \Delta t) \in \mathrm{T}_{\boldsymbol{\Phi}^0}\mathscr{C}$. Since $\Delta t \in \mathrm{T}_{t^0}\mathrm{S}^2$, the constraint condition $t^0 \cdot \Delta t = 0$ is identically satisfied by setting $\Delta t = \Lambda^0 \Delta T$, with $\Delta T \in \mathrm{T}_E\mathrm{S}^2$. A summary of the linear theory, along with matrix expressions relative to the standard basis ($\boldsymbol{E} \equiv \boldsymbol{E}_3$), is given in Table 1. Table 2 contains matrix expressions for the simplest example of an elastic isotropic constitutive model, as well as a higher-order constitutive model derived from an asymptotic expansion of the stored energy function for the three-dimensional linear theory.

3. Mixed variational formulation

As noted in Section 2.1 and in Part I of this work, the standard Galerkin formulation and, consequently, a displacement finite element implementation can be carried out entirely in curvilinear coordinates relative to the surface convected (Gaussian) frame $\{\boldsymbol{\varphi}_{,1}, \boldsymbol{\varphi}_{,2}, \boldsymbol{t}\}$. However, the mixed formulation set forth below requires the use of a local Cartesian frame in order to satisfy exact convergence requirements under constant strain fields. A simple procedure to construct this local Cartesian coordinate system is considered next.

3.1. Local Cartesian system in $T_{n^0}S^2$

Let $\boldsymbol{n}^0 = \boldsymbol{\varphi}^0_{,1} \times \boldsymbol{\varphi}^0_{,2} / \|\boldsymbol{\varphi}^0_{,1} \times \boldsymbol{\varphi}^0_{,2}\|$ be the normal field to the reference surface $\boldsymbol{\varphi}^0$: $\bar{\mathscr{A}} \to \mathbb{R}^3$. Define a local Cartesian system $\{x^a, x\}$, $a = 1, 2$, with base vectors $\{\boldsymbol{n}^0_1, \boldsymbol{n}^0_2, \boldsymbol{n}^0\}$ by means of the orthogonal transformation

$$\boldsymbol{\Lambda}^0_n = (\boldsymbol{E}_3 \cdot \boldsymbol{n}^0)\mathbf{1}_3 + \widehat{[\boldsymbol{E}_3 \times \boldsymbol{n}^0]} + \frac{1}{1 + \boldsymbol{E}_3 \cdot \boldsymbol{n}^0} (\boldsymbol{E}_3 \times \boldsymbol{n}^0) \otimes (\boldsymbol{E}_3 \times \boldsymbol{n}^0), \tag{3.1}$$

where

$$\boldsymbol{n}^0_a := \boldsymbol{\Lambda}^0_n \boldsymbol{E}_a \ (a = 1, 2) \quad \text{and} \quad \boldsymbol{n}^0 = \boldsymbol{\Lambda}^0_n \boldsymbol{E}_3 . \tag{3.2}$$

Observe that $\boldsymbol{\Lambda}^0_n$ maps $\boldsymbol{E}_3 \in S^2 \mapsto \boldsymbol{n}^0 := \boldsymbol{\Lambda}^0_n \boldsymbol{E}_3 \in S^2$ *without drill*, such that $\boldsymbol{\varphi}^0_{,\alpha} \cdot \boldsymbol{n}^0 = 0$. Since $\boldsymbol{n}^0_\alpha \cdot \boldsymbol{n}^0_b = \delta_{ab}$, and $\boldsymbol{n}^0 \cdot \boldsymbol{n}^0_a = 0$, by construction, we set

$$\frac{\partial x^a}{\partial \xi^\alpha} := \boldsymbol{n}^0_a \cdot \boldsymbol{\varphi}^0_{,\alpha} \ \Rightarrow \ \boldsymbol{\varphi}^0_{,\alpha} = \frac{\partial x^a}{\partial \xi^\alpha} \boldsymbol{n}^0_a . \tag{3.3a}$$

The transformation for partial differentiation then takes the standard form

$$\frac{\partial}{\partial \xi^\alpha} = \frac{\partial}{\partial x^\alpha} \frac{\partial x^a}{\partial \xi^\alpha} . \tag{3.3b}$$

We shall often make use of matrix notation. Accordingly, we set

$$\boldsymbol{J}_0 = \begin{bmatrix} \boldsymbol{n}^0_1 \cdot \boldsymbol{\varphi}^0_{,1} & \boldsymbol{n}^0_1 \cdot \boldsymbol{\varphi}^0_{,2} \\ \boldsymbol{n}^0_2 \cdot \boldsymbol{\varphi}^0_{,1} & \boldsymbol{n}^0_2 \cdot \boldsymbol{\varphi}^0_{,2} \end{bmatrix} . \tag{3.4}$$

Here and in following sections, derivatives relative to the coordinate functions of the local cartesian system $\{\boldsymbol{n}^0_1, \boldsymbol{n}^0_2, \boldsymbol{n}^0\}$ are denoted by $(\bullet)_{,a}$. For subsequent use, we note that the resultant strain measures in the Cartesian system take the form

$$\begin{aligned} \bar{\varepsilon}_{ab} &:= \tfrac{1}{2}(\boldsymbol{n}^0_a \cdot \boldsymbol{u}_{,b} + \boldsymbol{n}^0_b \cdot \boldsymbol{u}_{,a}) , \\ \bar{\kappa}_{ab} &:= \tfrac{1}{2}(\boldsymbol{n}^0_a \cdot \Delta \boldsymbol{t}_{,b} + \boldsymbol{n}^0_b \cdot \Delta \boldsymbol{t}_{,a} + \boldsymbol{u}_{,a} \cdot \boldsymbol{t}^0_{,b} + \boldsymbol{u}_{,b} \cdot \boldsymbol{t}^0_{,a}) , \\ \bar{\gamma}_a &:= \boldsymbol{n}^0_a \cdot \Delta \boldsymbol{t} + \boldsymbol{u}_{,a} \cdot \boldsymbol{t}^0 . \end{aligned} \tag{3.5}$$

Finally, making use of standard tensor transformations involving (3.3b), the constitutive equations for the effective stress resultants relative to the local cartesian system take the form

$$\tilde{n}^{ab} = \frac{Eh}{1 - \nu^2} H_0^{abcd} \bar{\varepsilon}_{cd} , \qquad \tilde{m}^{ab} = \frac{Eh^3}{12(1 - \nu^2)} H_0^{abcd} \bar{\kappa}_{cd} , \qquad \tilde{q}^a = \kappa G_s h \delta^{ab} \bar{\gamma}_b , \tag{3.6}$$

where

$$H_0^{abcd} = \nu \delta^{ab} \delta^{cd} + \frac{1 - \nu}{2} [\delta^{ac} \delta^{bd} + \delta^{ad} \delta^{cb}] , \tag{3.7}$$

and $\delta^{ab} = \delta_{ab} = \delta^a_b$ is the Kronecker delta.

3.2. Matrix notation: membrane and bending

The matrix formulation in the local Cartesian system is identical to that already considered for the curvilinear system. For completeness, we record below the basic results. Define:

$$\boldsymbol{u} := \begin{Bmatrix} u^1 \\ u^2 \\ u^3 \end{Bmatrix}, \qquad \bar{\boldsymbol{\varepsilon}} := \begin{Bmatrix} \bar{\varepsilon}_{11} \\ \bar{\varepsilon}_{22} \\ 2\bar{\varepsilon}_{12} \end{Bmatrix}, \qquad \bar{\boldsymbol{\kappa}} := \begin{Bmatrix} \bar{\kappa}_{11} \\ \bar{\kappa}_{22} \\ 2\bar{\kappa}_{12} \end{Bmatrix}, \qquad \Delta \boldsymbol{T} = \begin{Bmatrix} \Delta T^1 \\ \Delta T^2 \end{Bmatrix}. \tag{3.8}$$

Then, define $\mathbb{B}_m$: $[H^1(\bar{\mathscr{A}})]^3 \to [L^2(\bar{\mathscr{A}})]^3$ as

$$\mathbb{B}_m = \begin{bmatrix} \boldsymbol{n}_1^{0t} \dfrac{\partial}{\partial x^1} \\ \boldsymbol{n}_2^{0t} \dfrac{\partial}{\partial x^2} \\ \boldsymbol{n}_1^{0t} \dfrac{\partial}{\partial x^2} + \boldsymbol{n}_2^{0t} \dfrac{\partial}{\partial x^1} \end{bmatrix}. \tag{3.9}$$

In addition, define $\mathbb{B}_b \equiv [\mathbb{B}_{bm} \mathbb{B}_{bb}]$: $[H^1(\bar{\mathscr{A}})]^5 \to [L^2(\bar{\mathscr{A}})]^3$ by the expressions

$$\mathbb{B}_{bm} = \begin{bmatrix} \boldsymbol{t}_{,1}^{0t} \dfrac{\partial}{\partial x^1} \\ \boldsymbol{t}_{,2}^{0t} \dfrac{\partial}{\partial x^2} \\ \boldsymbol{t}_{,1}^{0t} \dfrac{\partial}{\partial x^2} + \boldsymbol{t}_{,2}^{0t} \dfrac{\partial}{\partial x^1} \end{bmatrix}, \qquad \mathbb{B}_{bb} = \begin{bmatrix} \boldsymbol{n}_1^{0t} \dfrac{\partial}{\partial x^1} \\ \boldsymbol{n}_2^{0t} \dfrac{\partial}{\partial x^2} \\ \boldsymbol{n}_1^{0t} \dfrac{\partial}{\partial x^2} + \boldsymbol{n}_2^{0t} \dfrac{\partial}{\partial x^1} \end{bmatrix} \bar{\boldsymbol{\Lambda}}^0, \tag{3.10}$$

where

$$\bar{\boldsymbol{\Lambda}}^0 := [\boldsymbol{t}_1^0 \quad \boldsymbol{t}_2^0] \equiv \begin{bmatrix} \Lambda_{11}^0 & \Lambda_{12}^0 \\ \Lambda_{21}^0 & \Lambda_{22}^0 \\ \Lambda_{31}^0 & \Lambda_{32}^0 \end{bmatrix}. \tag{3.11}$$

Finally set

$$\boldsymbol{H} = \begin{bmatrix} 1 & \nu & 0 \\ \nu & 1 & 0 \\ 0 & 0 & \dfrac{1-\nu}{2} \end{bmatrix}. \tag{3.12}$$

With this notation at hand, we have

$$\begin{aligned} \tilde{\boldsymbol{n}} &= \frac{Eh}{1-\nu^2} \boldsymbol{H} \bar{\boldsymbol{\varepsilon}}, \qquad \tilde{\boldsymbol{m}} = \frac{Eh^3}{12(1-\nu^2)} \boldsymbol{H} \bar{\boldsymbol{\kappa}}, \\ \bar{\boldsymbol{\varepsilon}} &= \mathbb{B}_m \boldsymbol{u}, \qquad \bar{\boldsymbol{\kappa}} = [\mathbb{B}_{bm} \mathbb{B}_{bb}] \begin{Bmatrix} \boldsymbol{u} \\ \Delta \boldsymbol{T} \end{Bmatrix}, \end{aligned} \tag{3.13}$$

where we have set $\tilde{\boldsymbol{n}} := [\tilde{n}^{11} \tilde{n}^{22} \tilde{n}^{12}]^t$ and $\tilde{\boldsymbol{m}} := [\tilde{m}^{11} \tilde{m}^{22} \tilde{m}^{12}]^t$.

3.3. Matrix notation transverse shear

Because the finite element treatment of the transverse shear strains employs an *assumed strain method*, it is more convenient to formulate the transverse shear strains relative to the surface convected basis $\{\boldsymbol{\varphi}^0_{,1}, \boldsymbol{\varphi}^0_{,2}, \boldsymbol{t}\}$. As is defined in Table 1, we set $\mathbb{B}_s \equiv [\mathbb{B}_{sm}\mathbb{B}_{sb}]$: $[H^1(\bar{\mathscr{A}})]^5 \to [L^2(\bar{\mathscr{A}})]^2$ as

$$\mathbb{B}_{sm} := \begin{bmatrix} \boldsymbol{t}_1^{0t} \dfrac{\partial}{\partial \xi^1} \\ \boldsymbol{t}_2^{0t} \dfrac{\partial}{\partial \xi^2} \end{bmatrix} \quad \text{and} \quad \mathbb{B}_{sb} := \begin{bmatrix} \boldsymbol{\varphi}^{0t}_{,1} \\ \boldsymbol{\varphi}^{0t}_{,2} \end{bmatrix} \bar{\boldsymbol{\Lambda}}^0 . \tag{3.14}$$

In addition, we set

$$\mathbb{C}_s = \kappa G_s h \begin{bmatrix} a^{0^{11}} & a^{0^{12}} \\ a^{0^{12}} & a^{0^{22}} \end{bmatrix}, \tag{3.15}$$

so that the transverse shear strains become:

$$\boldsymbol{\gamma} := \begin{Bmatrix} \gamma_1 \\ \gamma_2 \end{Bmatrix} = [\mathbb{B}_{sm}\mathbb{B}_{sb}] \begin{Bmatrix} \boldsymbol{u} \\ \Delta \boldsymbol{T} \end{Bmatrix} \tag{3.16}$$

and

$$\tilde{\boldsymbol{q}} := \begin{Bmatrix} \tilde{q}^1 \\ \tilde{q}^2 \end{Bmatrix} = \mathbb{C}_s \boldsymbol{\gamma} . \tag{3.17}$$

Next we consider the mixed variational formulation employed in the proposed linear shell model.

3.4. The mixed variational formulation

With the matrix notation introduced in the preceding sections, the linearized weak form of the momentum balance equations takes the form

$$G_{dyn} := B + \int_{\bar{\mathscr{A}}} [\bar{\rho}\ddot{\boldsymbol{u}} \cdot \boldsymbol{v} + \bar{I}_\rho \ddot{\Delta t} \cdot \delta t] \, d\mu^0 - G_{ext} , \tag{3.18}$$

where $\delta \boldsymbol{\Phi}^0 = (\boldsymbol{v}, \delta t) \in T_{\boldsymbol{\Phi}^0}\mathscr{C}$ is an arbitrary kinematical variation, and $d\mu^0 = \bar{j}^0 \, d\xi^1 \, d\xi^2$ is the reference surface measure,

$$G_{ext} := \int_{\bar{\mathscr{A}}} [\bar{\boldsymbol{n}} \cdot \boldsymbol{v} + \tilde{\bar{\boldsymbol{m}}} \cdot \delta t] \, d\mu^0 + \int_{\partial_n \bar{\mathscr{A}}} \bar{\bar{\boldsymbol{n}}} \cdot \boldsymbol{v} \bar{j} \, da^0 + \int_{\partial_m \bar{\mathscr{A}}} \bar{\bar{\boldsymbol{m}}} \cdot \delta t \bar{j} \, da^0 \tag{3.19}$$

is the virtual work of the external loading, and B is the *linearized static part* of the weak form of momentum balance, which takes the form

$$B := \int_{\bar{\mathscr{A}}} \left\{ [\mathbb{B}_m \boldsymbol{v}]^t \tilde{\boldsymbol{n}} + \left[[\mathbb{B}_{bm}\mathbb{B}_{bb}] \begin{pmatrix} \boldsymbol{v} \\ \delta \boldsymbol{T} \end{pmatrix} \right]^t \tilde{\boldsymbol{m}} + \left[[\mathbb{B}_{sm}\mathbb{B}_{sb}] \begin{pmatrix} \boldsymbol{v} \\ \delta \boldsymbol{T} \end{pmatrix} \right]^t \tilde{\boldsymbol{q}} \right\} d\mu^0 . \tag{3.20}$$

Here, we recall that *spatial* and *material* variations are connected through the relation $\delta t = \bar{\Lambda}^0\, \delta T$, where $t^0 = \Lambda^0 E$.

In addition to the weak form (3.20), we enforce the constitutive equations for the membrane and bending resultants through the variational forms:

$$G_M := \int_{\bar{\mathscr{A}}} \delta\tilde{n}^t \left[-\left(\frac{Eh}{1-\nu^2} H\right)^{-1} \tilde{n} + \mathbb{B}_m u \right] d\mu^0 = 0 , \tag{3.21}$$

where $\delta\tilde{n} \in [L^2(\bar{\mathscr{A}})]^3$, and

$$G_B := \int_{\bar{\mathscr{A}}} \delta\tilde{m}^t \left[-\left(\frac{Eh^3}{12(1-\nu^2)} H\right)^{-1} \tilde{m} + [\mathbb{B}_{bm}\mathbb{B}_{bb}] \begin{Bmatrix} u \\ \Delta T \end{Bmatrix} \right] d\mu^0 = 0 , \tag{3.22}$$

with $\delta\tilde{m} \in [L^2(\bar{\mathscr{A}})]^3$. The variational equations (3.20)–(3.22) constitute the basis for the finite element formulation discussed in detail in the following sections.

4. Finite element interpolations

The finite element interpolation of the reference surface φ^0: $\bar{\mathscr{A}} \to \mathbb{R}^3$ and the surface displacement field follows a standard procedure.

Let

$$\square := \{(\xi, \eta) \in [-1, 1] \times [-1, 1]\} \tag{4.1}$$

denote the biunit square, as shown in Fig. 1. According to the standard isoparametric concept, we define

$$\varphi_e^h : \square \to \mathbb{R}^3 , \qquad u_e^h : \square \to \mathbb{R}^3 \tag{4.2}$$

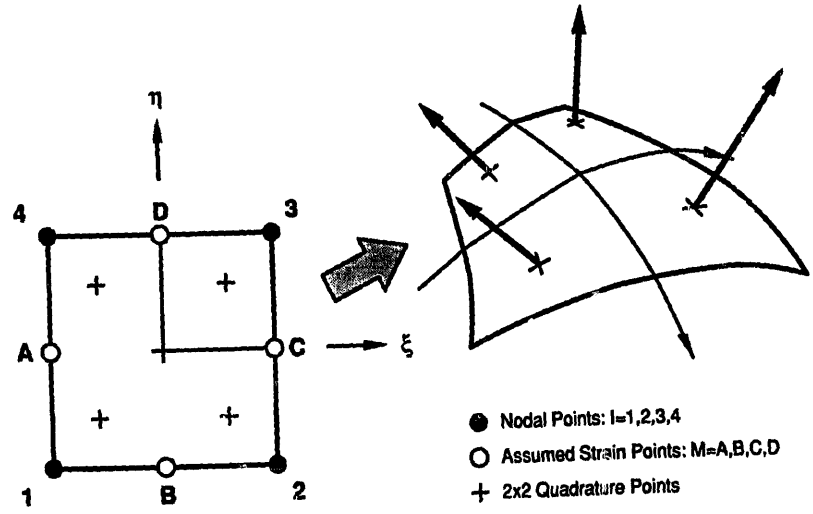

Fig. 1. Standard isoparametric biunit square, mapped into the shell element configuration.

by setting

$$\varphi_e^h := \sum_{I=1}^{4} N^I(\xi,\eta)\boldsymbol{d}_I\,, \tag{4.3a}$$

$$\boldsymbol{u}_e^h := \sum_{I=1}^{4} N^I(\xi,\eta)\boldsymbol{u}_I\,, \tag{4.3b}$$

where $\boldsymbol{d}_I \in \mathbb{R}^3$ and $\boldsymbol{u}_I \in \mathbb{R}^3$, $I = 1,\ldots,4$, and $N^I(\xi,\eta)$ are the standard bilinear isoparametric shape functions defined as

$$N^I(\xi,\eta) := \tfrac{1}{4}[1+\xi\xi_I][1+\eta\eta_I]\,, \quad I = 1,\ldots,4\,, \tag{4.4}$$

where $(\xi_I,\eta_I) \in \{(-1,-1);\,(1,-1);\,(1,1);\,(-1,1)\}$.

For further details on the isoparametric concept, we refer to standard references [17, 45].

The distinctive feature of the present approach concerns the interpolation of the *reference director field* t^0: $\bar{\mathscr{A}} \to \mathrm{S}^2$ and the *linearized director field* Δt: $\bar{\mathscr{A}} \to \mathrm{T}_t\mathrm{S}^2$. Crucial to the development of this interpolation is the geometric structure underlying the present shell model, which is considered in detail in Part I of this work. It will be shown below that the interpolation of the linearized director field is automatically defined and follows from the interpolation for the reference director field.

4.1. Reference director field

Let $\boldsymbol{t}_I^0 \in \mathrm{S}^2$ denote the directors (unit vectors) at the nodal points. Note that $\boldsymbol{t}^0_{I=1,\ldots,4}$ need not be normal to the reference mid-surface. Since t^0: $\bar{\mathscr{A}} \to \mathrm{S}^2$, we consider the following interpolation:

$$\boldsymbol{t}_e^h = \frac{\sum_{I=1}^{4} N^I \boldsymbol{t}_I^0}{\left\| \sum_{I=1}^{4} N^I \boldsymbol{t}_I^0 \right\|}\,. \tag{4.5}$$

This interpolation satisfies the geometric requirement that $\boldsymbol{t}_e^h \in \mathrm{S}^2$. For convenience, we introduce the notation

$$\tilde{\boldsymbol{t}}^h := \sum_{I=1}^{4} N^I \boldsymbol{t}_I^0 \;\Rightarrow\; \boldsymbol{t}_e^h \equiv \frac{\tilde{\boldsymbol{t}}^h}{\|\tilde{\boldsymbol{t}}^h\|}\,. \tag{4.6}$$

To simplify the notation, in what follows, the subindex "e" is often omitted.

4.1.1. Derivatives of the director field

In order to obtain the interpolation for the bending strain measures, one needs to calculate the derivatives of the reference director field. This is accomplished as follows.

Let $\mathbb{P}_t: \mathbb{R}^3 \to \mathrm{T}_t\mathrm{S}^2$ be the *orthogonal projection* defined as

$$\mathbb{P}_t := \mathbf{1}_3 - \boldsymbol{t} \otimes \boldsymbol{t} . \tag{4.7}$$

The fact that (4.7) defines an orthogonal projection follows from the properties:

(i) $\mathbb{P}_t = \mathbb{P}_t^{\mathrm{t}}$,

(ii) $\mathbb{P}_t \circ \mathbb{P}_t = \mathbb{P}_t \Rightarrow \mathbb{P}_t^N = \mathbb{P}_t \quad \forall N \in \mathbb{N}^+$,

(iii) $\mathbb{P}_t \boldsymbol{t} = \mathbf{0}$,

(iv) $\|\mathbb{P}_t\| := \max_{x \neq 0} \dfrac{\|\mathbb{P}_t x\|}{\|x\|} = 1$.

We now have the following

PROPOSITION 4.1. The derivative of $t^h: \bar{\mathscr{A}} \to \mathrm{S}^2$ *with respect to the surface coordinates is given by*

$$t^h_{,\alpha} = \frac{1}{\|\tilde{t}^h\|} \mathbb{P}_{t^h}\Big[\sum_{I=1}^{4} N^I_{,\alpha} t_I\Big] . \tag{4.8}$$

PROOF. By the chain rule

$$\begin{aligned} \frac{\partial \|\tilde{t}^h\|}{\partial \xi^\alpha} &= \frac{\partial}{\partial \xi^\alpha} \sqrt{\tilde{t}^h \cdot \tilde{t}^h} \\ &= \frac{1}{\|\tilde{t}^h\|} [\tilde{t}^h \cdot \tilde{t}^h_{,\alpha}] = t^h \cdot \tilde{t}_{,\alpha} . \end{aligned} \tag{4.9}$$

Therefore, from (4.6) we have

$$t^h_{,\alpha} = \frac{1}{\|\tilde{t}^h\|} [\tilde{t}^h_{,\alpha} - t^h (t^h \cdot \tilde{t}^h_{,\alpha})] , \tag{4.10}$$

and the result follows from definition (4.7). □

4.2. *Interpolation of the linearized director field*

To obtain the interpolation for the linearized director field *consistent with* (4.6), we use the property that $\Delta t^h: \bar{\mathscr{A}} \to \mathrm{T}_t\mathrm{S}^2$ *must take values in* $\mathrm{T}_t\mathrm{S}^2$. Consequently, we proceed as in the continuum problem (for further details, see Section 6 of Part I) and consider the curves

$$\varepsilon \mapsto \tilde{t}^h_\varepsilon := \sum_{I=1}^{4} N^I \exp_{t_I^0}[\varepsilon \, \Delta t_I] , \tag{4.11}$$

where

$$\exp_{t_I^0}[\varepsilon \, \Delta t_I] := \cos\|\varepsilon \, \Delta t_I\| t_I^0 + \frac{\sin\|\varepsilon \, \Delta t_I\|}{\|\varepsilon \, \Delta t_I\|} \varepsilon \, \Delta t_I \tag{4.12}$$

is the discrete exponential mapping at nodal points. Then, to obtain a curve $\varepsilon \mapsto t_\varepsilon^h \in S^2$, we set

$$\varepsilon \mapsto t_\varepsilon^h := \frac{\tilde{t}_\varepsilon}{\|\tilde{t}_\varepsilon\|} \in S^2 . \tag{4.13}$$

Construction (4.11)–(4.13) must satisfy two required properties:

(i) $t_\varepsilon^h|_{\varepsilon=0} = t^h \in S^2$,

(ii) $(\mathrm{d}/\mathrm{d}\varepsilon)|_{\varepsilon=0} t_\varepsilon^h =: \Delta t^h \in T_{t^h} S^2$.

Property (i) follows immediately from (4.11), (4.12), and (4.13). For property (ii) we have

$$\Delta t^h := \frac{\mathrm{d}}{\mathrm{d}\varepsilon}\bigg|_{\varepsilon=0} t_\varepsilon^h = \frac{1}{\|\tilde{t}^h\|} \mathbb{P}_{t^h} \Delta \tilde{t}^h , \tag{4.14}$$

where

$$\Delta \tilde{t}^h := \sum_{I=1}^{4} N^I \Delta t_I . \tag{4.15}$$

Therefore, by properties (i), (iii), and (iv) of $\mathbb{P}_{t^h}$,

$$t^h \cdot \mathbb{P}_{t^h} \Delta \tilde{t}^h = \mathbb{P}_{t^h}^{\mathrm{t}} t^h \cdot \Delta \tilde{t}^h \equiv 0 . \tag{4.16}$$

Thus, it follows that Δt^h as defined by (4.14), (4.15) is in $T_{t^0} S^2$. To summarize the results, we have the following.

PROPOSITION 4.2. The interpolation for the linearized director field consistent with (4.6) *is given by*

$$\Delta t^h = \frac{1}{\|\tilde{t}^h\|} \mathbb{P}_{t^h} \Delta \tilde{t}^h , \quad \textit{where } \Delta \tilde{t}^h := \sum_{I=1}^{4} N^I \Delta t_I . \tag{4.17}$$

4.2.1. Derivative of the linearized director field

We conclude this section by recording the counterpart of (4.8) for the director field. We have the following.

PROPOSITION 4.3. The derivative of the linearized director field is given by

$$\Delta t_{,\alpha}^h = \sum_{I=1}^{4} T_\alpha^I \Delta t_I , \tag{4.18}$$

where

$$T_\alpha^I := \frac{1}{\|\tilde{t}^h\|} \left\{ \mathbb{P}_{t^h} N_{,\alpha}^I - \left[t_{,\alpha}^h \otimes t^h + t^h \otimes t_{,\alpha}^h + \frac{1}{\|\tilde{t}^h\|} (t^h \cdot \tilde{t}_{,\alpha}^h) \mathbb{P}_{t^h} \right] N^I \right\} . \tag{4.19}$$

PROOF. The result follows immediately from (4.17) and by the chain rule with a calculation similar to that in Proposition 4.1. □

REMARKS 4.4. (1) Interpolation (4.5), (4.6) is only one among several possible approximation schemes. Alternatively, one may define

$$\tilde{t}_e^h = \sum_{I=1}^{4} N^I \exp[\bar{\chi}_I], \qquad t_e^h = \frac{\tilde{t}_e^h}{\|\tilde{t}_e^h\|}, \tag{4.20}$$

where $\bar{\chi}_I \in T_E S^2$; that is, $\bar{\chi}_I \cdot E = 0$. Observe that $\chi_I = E \times \bar{\chi}_I$ is the rotation vector of the director $t_I^0 \in S^2$. □

(2) Interpolation (4.20) requires the calculation of the rotation vector from $E \equiv E_3$ to t_I^0. This extraction requires a careful use of quaternions to avoid singularities [34, 35, 36]. For this reason, we advocate scheme (4.3), (4.6). □

(3) We recall that the transformation from *two rotational degrees of freedom* $\Delta T_I \in T_E S^2$ to a *three rotational degrees of freedom* $\Delta t_I \in T_{t^0} S^2$ is accomplished through the (3×2) matrix $\bar{\Lambda}_I^0$. This matrix constitutes the *first two columns* of

$$\Lambda_I^0 = (E \cdot t_I^0)\mathbf{1}_3 + \widehat{[E \times t_I^0]} + \frac{1}{1 + E \cdot t_I^0} (E \times t_I^0) \otimes (E \times t_I^0), \tag{4.21}$$

where $t_I^0 = \Lambda_I^0 E$. □

A summary of the interpolation procedure is contained in Table 3.

Table 3
Interpolation of the director field

1. Reference director field:

$$\tilde{t}_e^h := \sum_{I=1}^{4} N^I t_I^0 \Rightarrow t_e^h \equiv \frac{\tilde{t}_e^h}{\|\tilde{t}_e^h\|},$$

$$\Lambda_I^0 = (E \cdot t_I^0)\mathbf{1}_3 + \widehat{[E \times t_I^0]} + \frac{1}{1 + E \cdot t_I^0} (E \times t_I^0) \otimes (E \times t_I^0)$$

2. Derivatives (at Gauss points):

$$\mathbb{P}_{t^h} := \mathbf{1}_3 - t^h \otimes t^h,$$

$$\tilde{t}_{,\alpha}^h := \sum_{I=1}^{4} N_{,\alpha}^I t_I^0,$$

$$t_{,\alpha}^h = \frac{1}{\|\tilde{t}^h\|} \mathbb{P}_{t_h} \tilde{t}_{,\alpha}^h$$

3. Linearized director field: $\bar{\Lambda}_I^0 = [t_1^0 \; t_2^0]_I$,

$$\Delta t_I = \bar{\Lambda}_I^0 \Delta T_I,$$

$$\Delta t^h = \frac{1}{\|\tilde{t}^h\|} \mathbb{P}_{t^h} \sum_{I=1}^{4} N^I \Delta t_I,$$

$$T_\alpha^I := \frac{1}{\|\tilde{t}^h\|} \{\mathbb{P}_{t^h} N_{,\alpha}^I - [t_{,\alpha}^h \otimes t^h + t^h \otimes t_{,\alpha}^h + (t^h \cdot \tilde{t}_{,\alpha}^h)\mathbb{P}_{t^h}/\|\tilde{t}^h\|] N^I\},$$

$$\Delta t_{,\alpha}^h = \sum_{I=1}^{4} T_\alpha^I \Delta t_I$$

5. Treatment of membrane and bending strains

It is by now a well-established fact that strict adherance to the isoparametric concept for the membrane strain field, within the context of displacement-type approximations, results in poor performance of the finite element approximation. Stolarski and Belytschko [40, 41] coined the term *membrane locking* to characterize the inability of (fully integrated) displacement finite element interpolations to reproduce inextensional states of bending stress. Several schemes have been proposed to ameliorate this effect. These range from selective and uniform reduced integration techniques [13, 28, 46] to assumed strain methods [11, 18, 21, 27], and projection methods [6]. These methodologies appear to fall within the framework of mixed methods based on the Hu–Washizu principle [37]. Two observations concerning this class of methods should be made:

(i) A unified, sound, mathematical basis appears to be lacking, even within the context of plate theory. Recent attempts in this direction are made in [3, 4] among others. An exception to this unsatisfactory state of affairs is the recent work by Brezzi and Fortin [9] and Arnold and Falk [1].

(ii) In lieu of a more rigorous analysis, patch-test requirements [43] should be enforced. In this regard, we note that several variants of recently proposed assumed strain methods *do not pass* standard patch tests [18].

With these observations in mind, in this section we derive a treatment of the membrane and bending fields characterized by the following features:

(1) The treatment is consistent with a Hellinger–Reissner formulation. For *flat* plates, the interpolation procedure is closely related to the *mixed formulation* for plane stress proposed by Pian and Sumihara [29] (which appears to be optimal). The present formulation extends these ideas to shell elements with initial curvature.

(2) Correct rank: the element is free of spurious zero energy modes. In addition, exact satisfaction of patch test requirements is obtained.

(3) Excellent performance in standard numerical tests is achieved. The element appears to be free of membrane locking, and is among the top performers in the four-node element class.

5.1. Approximation for the membrane stresses

Let $\tilde{n}^{\alpha\beta}$ be the *convected components* of the *effective* membrane stresses. Accordingly:

$$\tilde{\boldsymbol{n}} = \tilde{n}^{\alpha\beta}\boldsymbol{\varphi}^0_{,\alpha} \otimes \boldsymbol{\varphi}^0_{,\beta} = \tilde{n}^{ab}\boldsymbol{n}^0_a \otimes \boldsymbol{n}^0_b \,. \tag{5.1}$$

The interpolation for the *Cartesian components*, $\tilde{n}^{ab}$, of the effective membrane resultant is constructed as follows:

(i) Assume interpolations, *discontinuous over elements*, of the form

$$[\tilde{n}^{ab}_e]^h = \begin{bmatrix} \bar{\beta}^e_1 & \bar{\beta}^e_3 \\ \bar{\beta}^e_3 & \bar{\beta}^e_2 \end{bmatrix} + \begin{bmatrix} \bar{\beta}^e_4(\eta - \bar{\eta}) & 0 \\ 0 & \bar{\beta}^e_5(\xi - \bar{\xi}) \end{bmatrix}, \tag{5.2}$$

where $\bar{\boldsymbol{\beta}}^e = [\bar{\beta}^e_1, \bar{\beta}^e_2, \bar{\beta}^e_3, \bar{\beta}^e_4, \bar{\beta}^e_5]^t \in \mathbb{R}^5$ and $\bar{\eta}, \bar{\xi} \in \mathbb{R}$ are constants to be specified below.

(ii) Let $\bar{J}_0 := J_0|_{\xi=\eta=0}$ be the Jacobian transformation from the basis $\{\bar{n}_1^0, \bar{n}_2^0\} \subset T_{\bar{n}^0}S^2$ to $\{\bar{\varphi}_{,1}^0, \bar{\varphi}_{,2}^0\} \subset T_{\bar{n}^0}S^2$. By (3.4), we have

$$\bar{J}_0 = \begin{bmatrix} \bar{n}_1^0 \cdot \bar{\varphi}_{,1}^0 & \bar{n}_1^0 \cdot \bar{\varphi}_{,2}^0 \\ \bar{n}_2^0 \cdot \bar{\varphi}_{,1}^0 & \bar{n}_2^0 \cdot \bar{\varphi}_{,2}^0 \end{bmatrix}, \tag{5.3a}$$

where $\bar{\varphi}_{,\alpha}^0 = \varphi_{,\alpha}^0|_{\xi=\eta=0}$ and $\bar{n}_a^0 = n_a^0|_{\xi=\eta=0}$.

Since the formulation is to be carried out in local Cartesian coordinates, the derivatives of the shape functions need to be transformed. This is accomplished by setting

$$\begin{Bmatrix} \tilde{N}_{,1}^I \\ \tilde{N}_{,2}^I \end{Bmatrix} = [J_0]^{-t} \begin{Bmatrix} N_{,\xi}^I \\ N_{,\eta}^I \end{Bmatrix}. \tag{5.3b}$$

(iii) The approximation for $\tilde{n}^{ab}$ is based on (5.2) and the coordinate transformation:

$$\tilde{n}^{ab} = \bar{J}_{0\alpha}^a \bar{J}_{0\beta}^a \tilde{n}^{\alpha\beta}, \tag{5.4}$$

where $\bar{J}_{0\alpha}^a$ are the components of $\bar{J}_0$.

This leads to the following finite-dimensional approximating subspace, S_n^h, for the effective membrane field

$$S_n^h := \left\{ \tilde{n}_e^h \in [L^2(\mathscr{A})]^3 \;\middle|\; \tilde{n}_e^h := \begin{Bmatrix} \tilde{n}^{11} \\ \tilde{n}^{22} \\ \tilde{n}^{12} \end{Bmatrix}_e = S(\xi,\eta)\beta_e,\ \beta_e \in \mathbb{R}^5 \right\}, \tag{5.5}$$

where

$$S(\xi,\eta) = [1_3 | (\eta - \bar{\eta})\bar{\mathscr{F}}_1 (\xi - \bar{\xi})\bar{\mathscr{F}}_2], \tag{5.6a}$$

with

$$\bar{\mathscr{F}}_1 = \begin{Bmatrix} (J_{01}^1)^2 \\ (J_{01}^2)^2 \\ J_{01}^1 J_{01}^2 \end{Bmatrix} \quad \text{and} \quad \bar{\mathscr{F}}_2 = \begin{Bmatrix} (J_{02}^1)^2 \\ (J_{02}^2)^2 \\ J_{02}^1 J_{02}^2 \end{Bmatrix}. \tag{5.6b}$$

(iv) Select $\bar{\xi}, \bar{\eta} \in \mathbb{R}$ by the expressions

$$\bar{\xi} = \frac{1}{\mathscr{A}_e} \int_{\bar{\Omega}} \xi \, d\mu^0, \qquad \bar{\eta} = \frac{1}{\mathscr{A}_e} \int_{\bar{\Omega}} \eta \, d\mu^0, \tag{5.7}$$

where $d\mu^0 = \bar{j}^0 \, d\xi \, d\eta$, and $\mathscr{A}_e = \int_{\bar{\Omega}} d\mu^0$.

REMARKS 5.1. (1) It is essential to perform the transformation (5.4) at the center of the element, otherwise patch test requirements *are violated.*

(2) The motivation for selecting $(\bar{\xi}, \bar{\eta})$ as in (5.7) lies in the simplicity of the resulting computational architecture. For plane stress, the method reduces to a one-point quadrature plus a rank-one stabilization, as in [7, 8]. The formulation in [29] corresponds to setting $\bar{\xi} = \bar{\eta} = 0$. □

A summary of the mixed interpolation parameters is contained in Table 4.

Table 4
Mixed formulation parameters

- Central Cartesian coordinate frame:

$$\bar{\boldsymbol{n}}^0 = \frac{\bar{\boldsymbol{\varphi}}^0_{,1} \times \bar{\boldsymbol{\varphi}}^0_{,2}}{\|\bar{\boldsymbol{\varphi}}^0_{,1} \times \bar{\boldsymbol{\varphi}}^0_{,2}\|},$$

$$\bar{\boldsymbol{A}}^0_n = [\bar{\boldsymbol{n}}^0_1\, \bar{\boldsymbol{n}}^0_2\, \bar{\boldsymbol{n}}^0]$$

$$= (\boldsymbol{E}_3 \cdot \bar{\boldsymbol{n}}^0)\mathbf{1}_3 + \widehat{[\boldsymbol{E}_3 \times \bar{\boldsymbol{n}}^0]} + \frac{1}{1 + \boldsymbol{E}_3 \cdot \bar{\boldsymbol{n}}^0}(\boldsymbol{E}_3 \times \bar{\boldsymbol{n}}^0) \otimes (\boldsymbol{E}_3 \times \bar{\boldsymbol{n}}^0)$$

- Jacobian transformation:

$$\bar{\boldsymbol{J}}_0 = \begin{bmatrix} \bar{\boldsymbol{n}}^0_1 \cdot \bar{\boldsymbol{\varphi}}^0_{,1} & \bar{\boldsymbol{n}}^0_1 \cdot \bar{\boldsymbol{\varphi}}^0_{,2} \\ \bar{\boldsymbol{n}}^0_2 \cdot \bar{\boldsymbol{\varphi}}^0_{,1} & \bar{\boldsymbol{n}}^0_2 \cdot \bar{\boldsymbol{\varphi}}^0_{,2} \end{bmatrix}$$

- Cartesian shape function derivatives:

$$\begin{Bmatrix} \tilde{N}^I_{,1} \\ \tilde{N}^I_{,2} \end{Bmatrix} = [\boldsymbol{J}^0]^{-1} \begin{Bmatrix} N^I_{,\xi} \\ N^I_{,\eta} \end{Bmatrix}$$

- Mixed interpolation:

$$\boldsymbol{S}(\xi, \eta) = [\mathbf{1}_3 | (\eta - \bar{\eta})\bar{\boldsymbol{\mathcal{F}}}_1 (\xi - \bar{\xi})\bar{\boldsymbol{\mathcal{F}}}_2],$$

$$\bar{\boldsymbol{\mathcal{F}}}_1 = \begin{Bmatrix} (\bar{\boldsymbol{J}}^1_{01})^2 \\ (\bar{\boldsymbol{J}}^2_{01})^2 \\ \bar{\boldsymbol{J}}^1_{01}\bar{\boldsymbol{J}}^2_{01} \end{Bmatrix}, \qquad \bar{\boldsymbol{\mathcal{F}}}_2 = \begin{Bmatrix} (\bar{\boldsymbol{J}}^1_{02})^2 \\ (\bar{\boldsymbol{J}}^2_{02})^2 \\ \bar{\boldsymbol{J}}^1_{02}\bar{\boldsymbol{J}}^2_{02} \end{Bmatrix},$$

$$\bar{\xi} = \frac{1}{\mathcal{A}_e}\int_{\bar{\Omega}} \xi \, \mathrm{d}\mu^0, \qquad \bar{\eta} = \frac{1}{\mathcal{A}_e}\int_{\bar{\Omega}} \eta \, \mathrm{d}\mu^0$$

5.1.1. *Matrix notation*

On the basis of the weak form (3.20), the contribution of the membrane stresses to the stiffness matrix is evaluated in a straightforward fashion as follows. Set

$$\boldsymbol{H}_{\mathrm{m}} := \int_{\bar{\Omega}} \boldsymbol{S}^{\mathrm{t}} \mathbb{C}_{\mathrm{m}}^{-1} \boldsymbol{S} \, \mathrm{d}\mu^0 . \tag{5.8}$$

Note that because of the choice (5.7), $\boldsymbol{H}_{\mathrm{m}}$ takes the simple form

$$\boldsymbol{H}_{\mathrm{m}} := \begin{bmatrix} \mathcal{A}_e \mathbb{C}_{\mathrm{m}}^{-1} & \boldsymbol{o}_{3\times 2} \\ \boldsymbol{o}_{2\times 3} & \bar{\boldsymbol{H}}_e \end{bmatrix}, \tag{5.9}$$

where $\bar{\boldsymbol{H}}_e$ is (2×2) matrix with the following structure. Let $\xi_1 = \xi$, $\xi_2 = \eta$, and

$$h_{\alpha\beta} = \int_{\bar{\Omega}} (\xi_\alpha - \bar{\xi}_\alpha)(\xi_\beta - \bar{\xi}_\beta) \, \mathrm{d}\mu^0 . \tag{5.10}$$

Then

$$\bar{H}_{e_{\alpha\beta}} = \bar{\mathscr{F}}^{t}_{\alpha}\mathbb{C}_{m}^{-1}\bar{\mathscr{F}}_{\beta}h_{\alpha\beta}\,, \tag{5.11}$$

where no sum on α, β is implied. Next compute

$$\boldsymbol{G}^{I}_{m} := \int_{\bar{\Omega}} \boldsymbol{S}^{t}_{e}[\boldsymbol{B}^{I}_{m}]\,d\mu^{0}\,, \tag{5.12}$$

where $[\boldsymbol{B}^{I}_{m}]$ is the discrete displacement approximation to the membrane strain-displacement operator (3.9) defined as

$$\boldsymbol{B}^{I}_{m} = \begin{bmatrix} \tilde{N}^{I}_{,1}\boldsymbol{n}^{0t}_{1} \\ \tilde{N}^{I}_{,2}\boldsymbol{n}^{0t}_{2} \\ \tilde{N}^{I}_{,1}\boldsymbol{n}^{0t}_{2} + \tilde{N}^{I}_{,2}\boldsymbol{n}^{0t}_{1} \end{bmatrix}. \tag{5.13}$$

Here, $\tilde{N}^{I}_{,\alpha}$ denote the derivatives of the shape functions relative to the *local Cartesian system*, which are computed using (5.3b).

The contribution of the membrane field to the stiffness matrix associated with nodes (I, J) is then given by

$$\boldsymbol{K}^{IJ}_{m} = [\boldsymbol{G}^{I}_{m}]^{t}\boldsymbol{H}^{-1}_{m}\boldsymbol{G}^{J}_{m}\,. \tag{5.14}$$

REMARKS 5.2.

(1) The inverse of $\boldsymbol{H}_{m}$ can be computed in closed form, because of the simple structure of equation (5.9).

(2) The product $[\boldsymbol{G}^{I}_{m}]^{t}\boldsymbol{H}^{-1}_{m}\boldsymbol{G}^{J}_{m}$ can be expanded and rephrased as a *one-point quadrature* plus stabilization; the one-point quadrature part being given by

$$\boldsymbol{B}^{I^{t}}_{0}\mathbb{C}_{m}\boldsymbol{B}^{J}_{0}\,, \qquad \boldsymbol{B}^{I}_{0} := \frac{1}{\mathscr{A}_{e}}\int_{\bar{\Omega}} \boldsymbol{B}^{I}_{m}\,d\mu^{0}\,, \tag{5.15}$$

which would be integrated using the central quadrature point. □

A summary of the membrane stiffness formulation is found in Table 5.

5.2. *Approximation of the bending stresses*

We start by recording the expressions for the discrete bending strain-displacement operator. By substituting interpolation (4.3) into (3.10), we obtain

$$\boldsymbol{B}^{I}_{bm} = \begin{bmatrix} \tilde{N}^{I}_{,1}\boldsymbol{t}^{0t}_{,1} \\ \tilde{N}^{I}_{,2}\boldsymbol{t}^{0t}_{,2} \\ \tilde{N}^{I}_{,1}\boldsymbol{t}^{0t}_{,2} + \tilde{N}^{I}_{,2}\boldsymbol{t}^{0t}_{,1} \end{bmatrix}, \tag{5.16}$$

Table 5
Membrane stiffness calculation

- Inverse constitutive matrix:

$$\mathbb{C}_{\mathrm{m}}^{-1} = \frac{1}{Eh}\begin{bmatrix} 1 & -\nu & 0 \\ -\nu & 1 & 0 \\ 0 & 0 & 2(1+\nu) \end{bmatrix}$$

- Strain-displacement matrix:

$$\boldsymbol{B}_{\mathrm{m}}^{I} = \begin{bmatrix} \tilde{N}_{,1}^{I}\boldsymbol{n}_1^{0\mathrm{t}} \\ \tilde{N}_{,2}^{I}\boldsymbol{n}_2^{0\mathrm{t}} \\ \tilde{N}_{,1}^{I}\boldsymbol{n}_2^{0\mathrm{t}} + \tilde{N}_{,2}^{I}\boldsymbol{n}_1^{0\mathrm{t}} \end{bmatrix}$$

- Mixed form:

$$\boldsymbol{H}_{\mathrm{m}}^{-1} = \left[\sum_{L=1}^{G-Pts} \boldsymbol{S}^{\mathrm{t}}\mathbb{C}_{\mathrm{m}}^{-1}\boldsymbol{S}\bar{j}_L^0 \mathcal{W}_L\right]^{-1},$$

$$\boldsymbol{G}_{\mathrm{m}}^{I} = \sum_{L=1}^{G-Pts} \boldsymbol{S}^{\mathrm{t}}\boldsymbol{B}_{\mathrm{m}}^{I}\bar{j}_L^0 \mathcal{W}_L$$

- Membrane stiffness:

$$\boldsymbol{K}_{\mathrm{m}}^{IJ} = \boldsymbol{G}_{\mathrm{m}}^{I\mathrm{t}}\boldsymbol{H}_{\mathrm{m}}^{-1}\boldsymbol{G}_{\mathrm{m}}^{J}$$

$$\boldsymbol{B}_{\mathrm{bb}}^{I} = \begin{bmatrix} \boldsymbol{n}_1^{0\mathrm{t}}\boldsymbol{T}_2^{I} \\ \boldsymbol{n}_2^{0\mathrm{t}}\boldsymbol{T}_2^{I} \\ (\boldsymbol{n}_2^{0\mathrm{t}}\boldsymbol{T}_1^{I} + \boldsymbol{n}_1^{0\mathrm{t}}\boldsymbol{T}_2^{I}) \end{bmatrix} \bar{\boldsymbol{A}}_I^0, \tag{5.17}$$

for $I = 1, \ldots, 4$, where $\boldsymbol{T}_\alpha^I$ is defined by (4.19). The interpolation of the curvatures then takes the form

$$\bar{\boldsymbol{\kappa}}_e^h = \begin{Bmatrix} \bar{\kappa}_{11} \\ \bar{\kappa}_{22} \\ 2\bar{\kappa}_{12} \end{Bmatrix}_e^h = \sum_{I=1}^{4} [\boldsymbol{B}_{\mathrm{bm}}^{I} | \boldsymbol{B}_{\mathrm{bb}}^{I}] \begin{Bmatrix} \boldsymbol{u}_I \\ \Delta\boldsymbol{T}_I \end{Bmatrix}. \tag{5.18}$$

At this point, two finite element approximation schemes are considered.

5.2.1. *Displacement formulation*

One simply enforces the bending constitutive equations *strongly* (or *point-wise*) through the relation

$$\tilde{\boldsymbol{m}}_e^h = \mathbb{C}_{\mathrm{b}}\bar{\boldsymbol{\kappa}}_e^h. \tag{5.19}$$

From (3.13), it follows that the contribution of the bending stress resultants to the stiffness matrix, associated with nodes (I, J) and denoted by $\boldsymbol{K}_{\mathrm{b}}^{IJ}$, is given by

$$\boldsymbol{K}_{\mathrm{b}}^{IJ} = \int_{\bar{\Omega}} \begin{Bmatrix} \boldsymbol{B}_{\mathrm{bm}}^{I^{\mathrm{t}}} \\ \boldsymbol{B}_{\mathrm{bb}}^{I^{\mathrm{t}}} \end{Bmatrix} \mathbb{C}_{\mathrm{b}} [\boldsymbol{B}_{\mathrm{bm}}^{J} \boldsymbol{B}_{\mathrm{bb}}^{J}] \, \mathrm{d}\mu^{0} \,. \tag{5.20}$$

5.2.2. *Mixed formulation*

Alternatively, one may enforce the constitutive equation (5.19) *weakly*, through variational equation (3.22). In particular, we consider the approximating subspace, S_{m}^{h}, of functions discontinuous between elements:

$$S_{\mathrm{m}}^{h} := \{\tilde{\boldsymbol{m}}_{e}^{h} \in [L^{2}(\mathscr{A})]^{3} \,|\, \tilde{\boldsymbol{m}}_{e}^{h} := \boldsymbol{S}(\xi, \eta)\boldsymbol{\alpha}_{e};\ \boldsymbol{\alpha}_{e} \in \mathbb{R}^{5}\} \,, \tag{5.21}$$

where $\boldsymbol{S}(\xi, \eta)$ is given by (5.6a). The implementation of this approach is entirely analogous to that considered in detail in Section 5.1 for the membrane stresses. The details are omitted, and a summary of the matrix formulation is presented in Table 6.

Table 6
Bending stiffness calculation (mixed form)

- Inverse constitutive matrix:

$$\mathbb{C}_{\mathrm{b}}^{-1} = \frac{12}{Eh^{3}} \begin{bmatrix} 1 & -\nu & 0 \\ -\nu & 1 & 0 \\ 0 & 0 & 2(1+\nu) \end{bmatrix}$$

- Strain-displacement matrix:

$$\boldsymbol{B}^{I^{\mathrm{b}}} = \left[\begin{array}{c|c} \tilde{N}_{,1}^{I} \boldsymbol{t}_{,1}^{0^{\mathrm{t}}} & \boldsymbol{n}_{1}^{0^{\mathrm{t}}} \boldsymbol{T}_{1}^{I} \bar{A}_{I}^{0} \\ \tilde{N}_{,2}^{I} \boldsymbol{t}_{,2}^{0^{\mathrm{t}}} & \boldsymbol{n}_{2}^{0^{\mathrm{t}}} \boldsymbol{T}_{2}^{I} \bar{A}_{I}^{0} \\ \tilde{N}_{,1}^{I} \boldsymbol{t}_{,2}^{0^{\mathrm{t}}} + \tilde{N}_{,2}^{I} \boldsymbol{t}_{,1}^{0^{\mathrm{t}}} & (\boldsymbol{n}_{2}^{0^{\mathrm{t}}} \boldsymbol{T}_{1}^{I} + \boldsymbol{n}_{1}^{0^{\mathrm{t}}} \boldsymbol{T}_{2}^{I}) \bar{A}_{I}^{0} \end{array}\right]$$

- Mixed form:

$$\boldsymbol{H}_{\mathrm{b}}^{-1} = \left[\sum_{L=1}^{G-Pts} \boldsymbol{S}^{\mathrm{t}} \mathbb{C}_{\mathrm{b}}^{-1} \boldsymbol{S} \bar{j}_{L}^{0} \mathscr{W}_{L} \right]^{-1},$$

$$\boldsymbol{G}_{\mathrm{b}}^{I} = \sum_{L=1}^{G-Pts} \boldsymbol{S}^{\mathrm{t}} \boldsymbol{B}_{\mathrm{b}}^{I} \bar{j}_{L}^{0} \mathscr{W}_{L}$$

- Bending stiffness:

$$\boldsymbol{K}_{\mathrm{b}}^{IJ} = \boldsymbol{G}_{\mathrm{b}}^{I^{\mathrm{t}}} \boldsymbol{H}_{\mathrm{b}}^{-1} \boldsymbol{G}_{\mathrm{b}}^{J}$$

6. Treatment of transverse shear strains

To avoid the *shear locking* phenomenon that dominates the performance of displacement finite element formulations in the thin shell limit, we employ an *assumed strain method* based on the Hu–Washizu principle. The construction of the assumed covariant shear strain interpolation is closely related to procedures advocated by MacNeal [21], Hughes and Tezduyar [16], Bathe and Dvorkin [5]. The only available mathematical analysis of this scheme is due to Bathe and Brezzi [3, 4].

Here, we cast the approximation scheme in the context of a Hu–Washizu type of variational principle following ideas of Simo and Hughes [37].

6.1. Construction of the assumed strain field

Consider a typical isoparametric finite element, as depicted in Fig. 2, and denote by $M = A, B, C, D$, the set of mid-points of the element boundaries. Following MacNeal [21] and Bathe and Dvorkin [5], we consider the following assumed transverse shear strain field:

$$\bar{\gamma}_1^h = \tfrac{1}{2}[(1-\eta)\gamma_1^B + (1+\eta)\gamma_1^D], \tag{6.1a}$$

$$\bar{\gamma}_2^h = \tfrac{1}{2}[(1-\xi)\gamma_2^A + (1+\xi)\gamma_2^C], \tag{6.1b}$$

where

$$\gamma_2^A = \boldsymbol{t}^A \cdot \boldsymbol{u}_{,2}^A + \Delta\boldsymbol{t}^A \cdot \boldsymbol{\varphi}_{,2}^A, \tag{6.2a}$$

$$\gamma_1^B = \boldsymbol{t}^B \cdot \boldsymbol{u}_{,1}^B + \Delta\boldsymbol{t}^B \cdot \boldsymbol{\varphi}_{,1}^B, \tag{6.2b}$$

$$\gamma_2^C = \boldsymbol{t}^C \cdot \boldsymbol{u}_{,2}^C + \Delta\boldsymbol{t}^C \cdot \boldsymbol{\varphi}_{,2}^C, \tag{6.2c}$$

$$\gamma_1^D = \boldsymbol{t}^D \cdot \boldsymbol{u}_{,1}^D + \Delta\boldsymbol{t}^D \cdot \boldsymbol{\varphi}_{,1}^D \tag{6.2d}$$

are the covariant transverse shear strains collocated at the midpoints of the element boun-

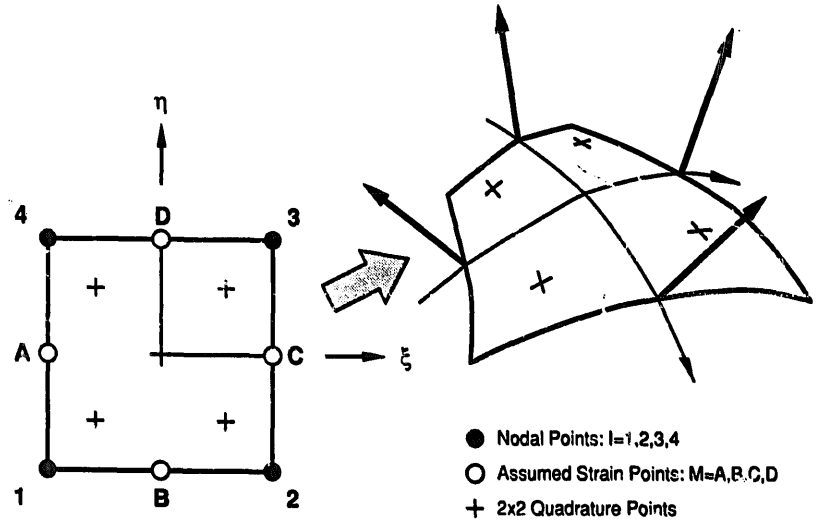

Fig. 2. Construction of the assumed strain field on the standard isoparametric biunit square.

daries. Making use of interpolation (4.3), it follows that

$$\begin{aligned} \boldsymbol{\varphi}^A_{,2} &= \tfrac{1}{2}(\boldsymbol{d}_4 - \boldsymbol{d}_1)\,, \qquad \boldsymbol{\varphi}^C_{,2} = \tfrac{1}{2}(\boldsymbol{d}_3 - \boldsymbol{d}_2)\,, \\ \boldsymbol{\varphi}^B_{,1} &= \tfrac{1}{2}(\boldsymbol{d}_2 - \boldsymbol{d}_1)\,, \qquad \boldsymbol{\varphi}^D_{,1} = \tfrac{1}{2}(\boldsymbol{d}_3 - \boldsymbol{d}_4)\,. \end{aligned} \tag{6.3}$$

Similar expressions are obtained for the surface displacement field $\boldsymbol{u}^h_e$: $\square \mapsto \mathbb{R}^3$.

Next, from the assumed interpolation of the director field given by (4.5), we obtain

$$\boldsymbol{t}^M = \frac{\boldsymbol{t}^0_\alpha + \boldsymbol{t}^0_\beta}{\|\boldsymbol{t}^0_\alpha + \boldsymbol{t}^0_\beta\|}\,, \quad \begin{cases} M = A, B, C, D\,, \\ \alpha = 1, 2, 3, 4\,, \\ \beta = 4, 1, 2, 3\,. \end{cases} \tag{6.4}$$

Finally, we note that

$$\boldsymbol{\varphi}^0_{,\alpha} \cdot \frac{1}{\|\tilde{\boldsymbol{t}}^h\|}\,\mathbb{P}_{t^h}\,\Delta\tilde{\boldsymbol{t}} = \frac{1}{\|\tilde{\boldsymbol{t}}^h\|}\,\mathbb{P}_{t^h}\boldsymbol{\varphi}^0_{,\alpha} \cdot \Delta\tilde{\boldsymbol{t}} \equiv \boldsymbol{\eta}_\alpha \cdot \Delta\tilde{\boldsymbol{t}}\,, \tag{6.5}$$

where $\boldsymbol{\eta}_\alpha = (1/\|\tilde{\boldsymbol{t}}^h\|)\mathbb{P}_{t^h}\boldsymbol{\varphi}^0_{,\alpha}$. Recalling the properties of the projection operator $\mathbb{P}_{t^h}: \mathbb{R}^3 \to \mathrm{T}_t\mathrm{S}^2$, and making use of (4.17), the second term in (6.2a) now becomes:

$$\Delta\boldsymbol{t}^A \cdot \boldsymbol{\varphi}^A_{,2} = \frac{\Delta\boldsymbol{t}_1 + \Delta\boldsymbol{t}_4}{2} \cdot \boldsymbol{\eta}^A_2\,. \tag{6.6a}$$

In this expression, $\boldsymbol{\eta}^A_2$ is defined as

$$\boldsymbol{\eta}^A_2 := \frac{1}{\|\tilde{\boldsymbol{t}}^A\|}\,\mathbb{P}_{t^A}\boldsymbol{\varphi}^A_{,2} = \frac{\boldsymbol{\varphi}^A_{,2} - (\boldsymbol{\varphi}^A_{,2} \cdot \boldsymbol{t}^A)\boldsymbol{t}^A}{\|\tfrac{1}{2}(\boldsymbol{t}^0_1 + \boldsymbol{t}^0_4)\|}\,. \tag{6.6b}$$

Similar expressions are readily derived for the remaining terms in (6.2).

By making use of the relations (6.2)–(6.6), the assumed covariant transverse shear field may be expressed as follows. Set

$$\boldsymbol{u}_e := \begin{Bmatrix} \boldsymbol{u}_1 \\ \boldsymbol{u}_2 \\ \boldsymbol{u}_3 \\ \boldsymbol{u}_4 \end{Bmatrix} \in \mathbb{R}^{12}\,, \qquad \Delta\boldsymbol{T}_e := \begin{Bmatrix} \Delta\boldsymbol{T}_1 \\ \Delta\boldsymbol{T}_2 \\ \Delta\boldsymbol{T}_3 \\ \Delta\boldsymbol{T}_4 \end{Bmatrix} \in \mathbb{R}^8\,. \tag{6.7}$$

Then

$$\bar{\boldsymbol{\gamma}}^h_e \equiv \begin{Bmatrix} \bar{\gamma}^h_1 \\ \bar{\gamma}^h_2 \end{Bmatrix}_e := \bar{\boldsymbol{B}}_{\mathrm{sm}}\boldsymbol{u}_e + \bar{\boldsymbol{B}}_{\mathrm{sb}}\,\Delta\boldsymbol{T}_e\,, \tag{6.8}$$

where

$$\bar{\boldsymbol{B}}_{\mathrm{sm}} := \tfrac{1}{4}\begin{bmatrix} -(1-\eta)\boldsymbol{t}^{B^t} & (1-\eta)\boldsymbol{t}^{B^t} & (1+\eta)\boldsymbol{t}^{D^t} & -(1+\eta)\boldsymbol{t}^{D^t} \\ -(1-\xi)\boldsymbol{t}^{A^t} & -(1+\xi)\boldsymbol{t}^{C^t} & (1+\xi)\boldsymbol{t}^{C^t} & (1-\xi)\boldsymbol{t}^{A^t} \end{bmatrix} \tag{6.9}$$

and

$$\bar{\boldsymbol{B}}_{\mathrm{sb}} := \tfrac{1}{4}\begin{bmatrix} (1-\eta)\boldsymbol{\eta}^{B^t}_1 & (1-\eta)\boldsymbol{\eta}^{B^t}_1 & (1+\eta)\boldsymbol{\eta}^{D^t}_1 & (1+\eta)\boldsymbol{\eta}^{D^t}_1 \\ (1-\xi)\boldsymbol{\eta}^{A^t}_2 & (1+\xi)\boldsymbol{\eta}^{C^t}_2 & (1+\xi)\boldsymbol{\eta}^{C^t}_2 & (1-\xi)\boldsymbol{\eta}^{A^t}_2 \end{bmatrix} \bar{\boldsymbol{\Pi}}^0\,. \tag{6.10a}$$

Here, $\bar{\boldsymbol{\Pi}}^0$ is a (12×8) transformation matrix defined as

$$\bar{\boldsymbol{\Pi}}^0 = \begin{bmatrix} \bar{\boldsymbol{\Lambda}}_1^0 & & & \\ & \bar{\boldsymbol{\Lambda}}_2^0 & & \\ & & \bar{\boldsymbol{\Lambda}}_3^0 & \\ & & & \bar{\boldsymbol{\Lambda}}_4^0 \end{bmatrix}. \tag{6.10b}$$

This completes the development of the assumed strain field $\bar{\boldsymbol{\gamma}}^h$. The discrete variational formulation is constructed on the basis of the following mixed principle.

6.2. Mixed HU–Washizu formulation

Let

$$\Pi_s := \int_{\bar{\Omega}} [\tfrac{1}{2}\bar{\boldsymbol{\gamma}}^h \cdot \mathbb{C}_s \bar{\boldsymbol{\gamma}}^h + \tilde{\boldsymbol{q}}^h(\boldsymbol{\gamma}^h - \bar{\boldsymbol{\gamma}}^h)]\, d\mu^0 \tag{6.11}$$

be the potential energy associated with the transverse shear strain, expressed in a Hu–Washizu form. Here $\bar{\boldsymbol{\gamma}}^h$ denotes the assumed transverse shear strain field, and $\boldsymbol{\gamma}^h$ is the shear strain field emanating from the isoparametric interpolation; accordingly:

$$\boldsymbol{\gamma}_e^h = \boldsymbol{B}_{sm}\boldsymbol{u}_e + \boldsymbol{B}_{sb}\,\Delta\boldsymbol{T}_e\,, \tag{6.12}$$

where $\boldsymbol{B}_{sm}$ and $\boldsymbol{B}_{sb}$ are obtained from (3.14) and by interpolations (4.3), (4.6), and (4.17). The first variation of (6.11) relative to $(\boldsymbol{v}^h, \delta\boldsymbol{t}^h) \in \mathbb{R}^3 \times T_{t^0}S^2$ then yields the contribution of the transverse shear strain field of the weak form (3.20) as

$$G_s := \int_{\bar{\Omega}} \left[[\bar{\boldsymbol{B}}_{sm}\bar{\boldsymbol{B}}_{sb}] \begin{Bmatrix} \boldsymbol{v}^h \\ \delta\boldsymbol{T}^h \end{Bmatrix} \right]^t \tilde{\boldsymbol{q}}^h\, d\mu^0\,. \tag{6.13}$$

This expression is identical to that in (3.20) with $[\boldsymbol{B}_{sm}\boldsymbol{B}_{sb}]$ replaced by the assumed strain operator $[\bar{\boldsymbol{B}}_{sm}\bar{\boldsymbol{B}}_{sb}]$. In addition to (6.13), from (6.11) one obtains the following two variational equations:

$$\int_{\bar{\Omega}} (\delta\tilde{\boldsymbol{q}}^h)^t([\boldsymbol{B}_{sm}\boldsymbol{B}_{sb}] - [\bar{\boldsymbol{B}}_{sm}\bar{\boldsymbol{B}}_{sb}])\, d\mu^0 \begin{Bmatrix} \boldsymbol{u}^h \\ \Delta\boldsymbol{T}^h \end{Bmatrix} = 0 \tag{6.14}$$

and

$$[\boldsymbol{v}^h\ \delta\boldsymbol{T}^h] \int_{\bar{\Omega}} \begin{Bmatrix} \bar{\boldsymbol{B}}_{sm}^t \\ \bar{\boldsymbol{B}}_{sb}^t \end{Bmatrix} \left(-\mathbb{C}_s[\bar{\boldsymbol{B}}_{sm}\bar{\boldsymbol{B}}_{sb}] \begin{Bmatrix} \boldsymbol{u}^h \\ \Delta\boldsymbol{T}^h \end{Bmatrix} + \tilde{\boldsymbol{q}}^h \right) d\mu^0 = 0\,, \tag{6.15}$$

for arbitrary $\delta\tilde{\boldsymbol{q}}^h \in [L^2(\bar{\mathscr{A}})]^2$ and $(\boldsymbol{v}_e, \delta\boldsymbol{T}_e) \in \mathbb{R}^3 \times T_E S^2$. It can be shown (see [37] that $\tilde{\boldsymbol{q}}^h$ can always be chosen such that (6.14) and (6.15) are satisfied, and (6.13) takes the form

$$G_s = [\boldsymbol{v}^t\ \delta\boldsymbol{T}^t] \int_{\bar{\Omega}} \begin{Bmatrix} \bar{\boldsymbol{B}}_{sm}^t \\ \bar{\boldsymbol{B}}_{sb}^t \end{Bmatrix} \mathbb{C}_s[\bar{\boldsymbol{B}}_{sm}\bar{\boldsymbol{B}}_{sb}]\, d\mu^0 \begin{Bmatrix} \boldsymbol{u}_e \\ \Delta\boldsymbol{T}_e \end{Bmatrix}. \tag{6.16}$$

In other words; the approximation procedure can be formulated as a $\bar{\boldsymbol{B}}$-method as proposed in

Table 7
Shear stiffness calculation

- Constitutive matrix:

$$\mathbb{C}_s = \kappa G_s h \begin{bmatrix} a^{0\,11} & a^{0\,12} \\ a^{0\,21} & a^{0\,22} \end{bmatrix}$$

- Strain-displacement matrix (see (6.2)–(6.6)):

$$\bar{B}_s = \left[\begin{array}{c|c||c|c} N^1_{,1}\boldsymbol{t}^t_B & N^2_{,1}\boldsymbol{\eta}^B_{,1}\cdot\bar{\Lambda}_1 & N^2_{,1}\boldsymbol{t}^t_B & N^2_{,1}\boldsymbol{\eta}^B_{,1}\cdot\bar{\Lambda}_2 \\ N^1_{,2}\boldsymbol{t}^t_A & N^1_{,2}\boldsymbol{\eta}^A_{,2}\cdot\bar{\Lambda}_1 & N^2_{,2}\boldsymbol{t}^t_C & N^3_{,2}\boldsymbol{\eta}^C_{,2}\cdot\bar{\Lambda}_2 \\ \hline\hline N^3_{,1}\boldsymbol{t}^t_D & N^3_{,1}\boldsymbol{\eta}^D_{,1}\cdot\bar{\Lambda}_3 & N^4_{,1}\boldsymbol{t}^t_D & N^3_{,1}\boldsymbol{\eta}^D_{,1}\cdot\bar{\Lambda}_4 \\ N^3_{,2}\boldsymbol{t}^t_C & N^3_{,2}\boldsymbol{\eta}^C_{,2}\cdot\bar{\Lambda}_3 & N^4_{,2}\boldsymbol{t}^t_A & N^4_{,2}\boldsymbol{\eta}^A_{,2}\cdot\bar{\Lambda}_4 \end{array}\right]$$

- Shear stiffness:

$$\boldsymbol{K}^{IJ}_s = \sum_{L=1}^{G-Pts} \bar{\boldsymbol{B}}^{I\,t}_s \mathbb{C}_s \bar{\boldsymbol{B}}^J_s \bar{j}^0_L W_L$$

[12]. We note that the interpolation scheme advocated in [16] falls within this class of methods. Consequently, the contribution of the transverse shear strains to the stiffness matrix becomes

$$\boldsymbol{K}_s|_e := \int_{\bar{\Omega}} \begin{Bmatrix} \bar{\boldsymbol{B}}^t_{sm} \\ \bar{\boldsymbol{B}}^t_{sb} \end{Bmatrix} \mathbb{C}_s [\bar{\boldsymbol{B}}_{sm} \bar{\boldsymbol{B}}_{sb}] \, d\mu^0 . \tag{6.17}$$

A summary of the matrix formulation of the assumed-strain shear stiffness is found in Table 7.

7. Numerical simulations

The performance of the proposed shell element is evaluated with several discriminating problems selected from the literature. Patch tests for the constant states of stress of the element are first listed, then some of the more challenging problems suggested by MacNeal and Harder [22], Liu et al. [19], and Stanley [38] are performed. Problems examining sensitivity of the element to mesh distortion are also examined. The convergence of the results is compared to other well-known formulations ranging from four-node discrete Kirchoff approximations to biquadratic *degenerated solid* formulations. A listing of these shell elements, and the abbreviations used to identify them henceforth, is contained in Table 8.

7.1. The patch test

A square plate is modeled using the single element shown in Fig. 3(a) and the skewed mesh shown in Fig. 3(b), and subjected to constant states of tension and bending. The stresses and

Table 8
Listing of some standard shell elements

Name	Description
4-ANS	bilinear assumed natural strain element, with full integration Stanley [38], Parks and Stanley [27]
4-CBS	bilinear continuum based shell element of Bathe and Brezzi [3]
4-DKQ	discrete Kirchoff quadrilateral of Taylor [42]
4-RSDS	bilinear resultant-stress degenerated-shell element, with uniform reduced integration and stabilization Liu et al. [19]
4-SRI	bilinear degenerated shell element, with selective reduced integration Hughes and Liu [15]
4-URI	bilinear uniformly reduced Lagrangian degenerated shell
9-ANS	biquadratic assumed natural strain element, with full integration Stanley [38], Parks and Stanley [27]
9-GAMMA	biquadratic degenerated shell element, with uniform reduced integration and γ stabilization Belytchko et al. [6]
9-SRI	biquadratic degenerated shell element, with selective reduced integration
T1	bilinear plate bending element of Hughes and Tezduyar [16]
Present formulations:	
MIXED	bilinear shell described in the previous sections with the *mixed* formulation used for the membrane and bending stresses and full 2×2 quadrature
DISP	bilinear shell described in the previous sections with the *displacement* formulation used for the membrane and bending stresses and full 2×2 quadrature

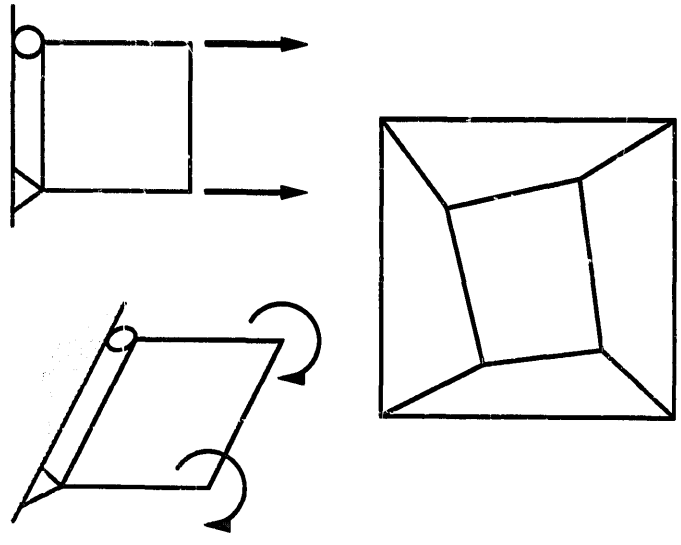

Fig. 3. Constant stress patch tests: Tension, bending, and in-plane twist

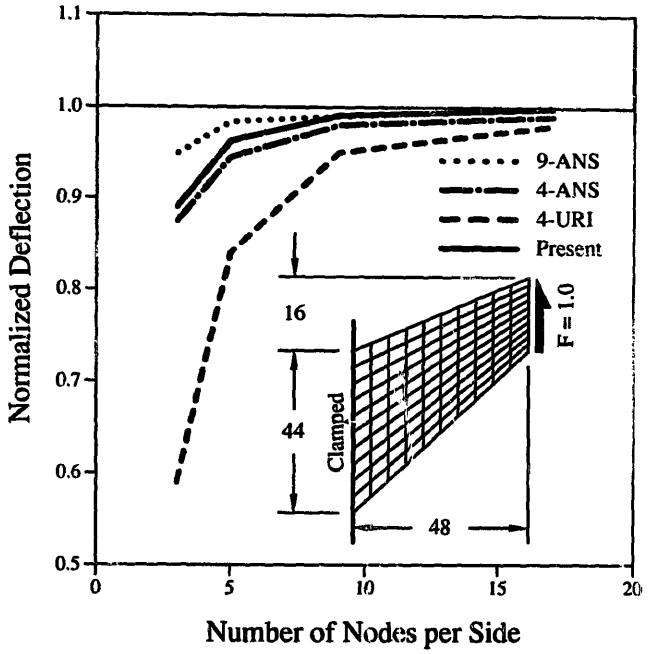

Fig. 4. Description and results of Cook's membrane problem. Present results are for the mixed formulation.

displacements obtained with both meshes are exactly identical to the analytical answers. The material and geometric properties are: $E = 10 \times 10^6$, $\nu = 0.3$, and $l = 10$.

7.2. *Cook's membrane problem*

A trapezoidal plate is clamped on one end and subjected to a distributed in-plane bending load on the other end, as shown in Fig. 4. This problem has a considerable amount of shear deformation, and is an excellent test of an element's ability to model membrane dominated situations with skewed meshes. A finite element converged solution of 23.91 is used to normalize the results, which are shown in Fig. 4 and listed in Table 9. The material properties are $E = 1.0$, $\nu = 0.33$, and $h = 1.0$. The proposed element's performance surpasses the bi-linear shell elements and is among the ranks of the biquadratic elements. 70% of the final solution is captured with one single element.

Table 9
Results of Cook's membrane problem

Number of Elements	Displacements (inches)	(%)
1	16.743	70.0
4	21.124	88.3
16	23.018	96.3
64	23.685	99.1
256	23.878	99.9

7.3. Bending of a rhombic plate

A simply supported rhombic plate of side $l = 100$, material properties $E = 10 \times 10^6$, $\nu = 0.3$, and thickness $h = 1.0$ is uniformly pressure loaded. The centerpoint deflection is normalized with the analytical solution of 0.04455, obtained by Morely [23, 24].

The difficulty in this problem arises from the singularity of the solution at the obtuse vertices, where the stresses tend to infinity, and thus the usefulness of this problem has been questioned. To alleviate some of the numerical difficulties, several different mesh configurations have been used. Hughes [17] uses a uniform mesh on a quadrant of the problem with smaller elements at the base, which yields elements of trapezoidal shape. Vu-Quoc and Mora [44] use a uniform nine-node element mesh, but move the interior nodal points closer to the obtuse vertex. To assess the convergence of shell elements of different configurations, we use the uniform mesh shown in Fig. 5. This mesh is a more demanding configuration due to the rhombic shape of the elements and the lack of mesh refinement at the singularity points.

Again, the proposed element proves to be superior to other bilinear formulations, and in this case even to the biquadratic elements. Stanley [38] reports that the 4-SRI element initially gives good answers, however it diverges from the correct answer as the mesh is refined. The results are listed in Table 10 and shown in Fig. 5. The superior performance of the element is attributed to the mixed formulation used for the bending stresses. When the displacement formulation is used for the bending, the results are identical to the 4-CBS and T1 elements.

7.4. Shearing of a twisted ribbon

This problem, a *beam* twisted 90°, was suggested by MacNeal and Harder [22] as a test to assess the effect of warping on the performance of a shell element. A more demanding version

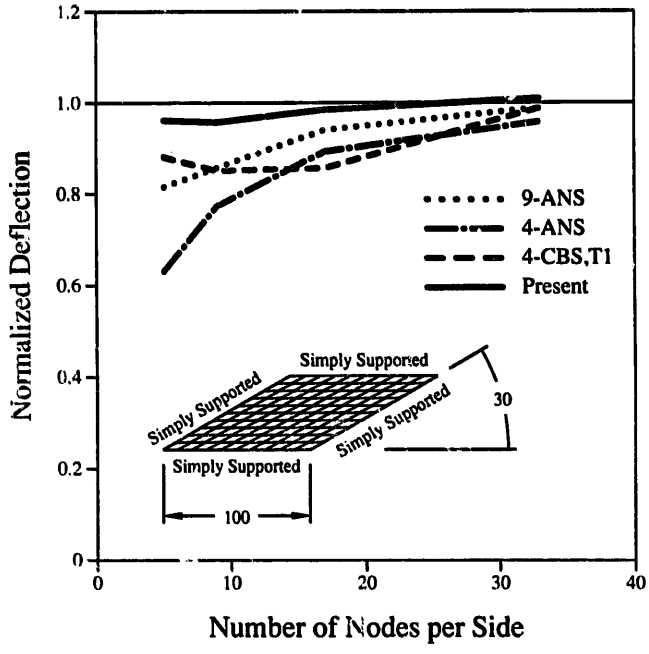

Fig. 5. Description and results of the rhombic plate under uniform presure loading. Present results are for the mixed formulation.

Table 10
Results of the rhombic plate

Nodes per side	Center displacement (inches)	(%)
5	0.04282	96.1
9	0.04264	95.7
17	0.04387	98.5
33	0.04496	100.9

Table 11
Results of the twisted ribbon

Mesh size	Load case (a) (inches)	(%)	Load Case (b) (inches)	(%)
1 × 6	1.378	99.1	0.3261	95.1
2 × 12	1.387	99.8	0.3383	98.6
4 × 24	1.389	99.9	0.3421	99.7
8 × 48	1.390	100.0	0.3431	100.0

of the same problem (used here) is obtained for the case of a *twisted thin shell*. A thin shell of length $l = 12$, width $w = 1.1$, thickness $t = 0.05$, and material properties $E = 29.0 \times 10^6$, $\nu = 0.22$, twisted by 90° is cantilevered and subjected to two cases of end loading:

(a) Unit shear load in the *width* direction.

(b) Unit shear load in the *thickness* direction.

The results are listed in Table 11 and shown in Fig. 6. The proposed element encounters no difficulties in modeling this problem effectively even with coarse meshes.

7.5. *Pinched hemispherical shell*

A pinched hemispherical shell, with two inward and two outward forces 90° apart is modeled using symmetry boundary conditions on one quadrant. This problem is a good test of the inextensional bending behavior of an element, and an excellent test for the ability of an element to model rigid-body motions.

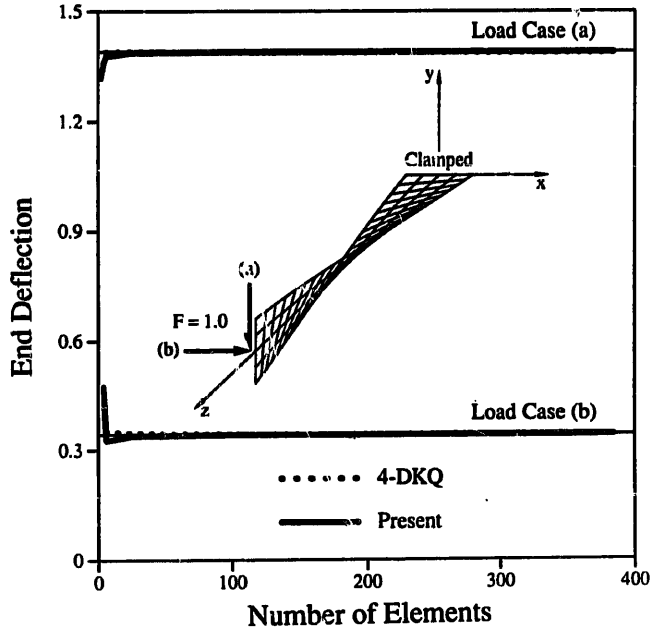

Fig. 6. Description and results of the twisted ribbon under two cases of shear loading: (a) in the width direction, (b) in the thickness direction. Present results are for the mixed formulation.

Table 12
Normalized results of the pinched hemisphere with 18° hole

Nodes per side	Mixed (%)	4-DKQ (%)
3	91.9	66.3
5	100.4	92.8
9	99.8	101.0
17	99.9	100.3

Two separate problems have traditionally been used to evaluate the performance of elements: the pinched hemisphere with an 18° hole at the top, shown in Fig. 7, and the full pinched hemisphere, shown in Fig. 8. Both problems share the same material properties: $E = 6.825 \times 10^7$ and $\nu = 0.3$, radius $R = 10$, and thickness $h = 0.04$.

7.5.1. *Hemispherical shell with 18° hole*

A value of 0.094 has been published [22] for the displacement at the points of application of the forces, however, analytical solutions based on asymptotic expansions [39] appear to yield an answer of 0.093, which is used for the normalization. Table 12 lists the results of this problem and Fig. 7 compares the proposed element's performance to the 4-DKQ, 9-SRI, and 9-GAMMA elements.

The performance of the proposed element in this problem is quite remarkable. A mere 2×2 mesh produces 92% of the numerical answer, and the results are practically converged with the 4×4 mesh. No shear or membrane locking is detected.

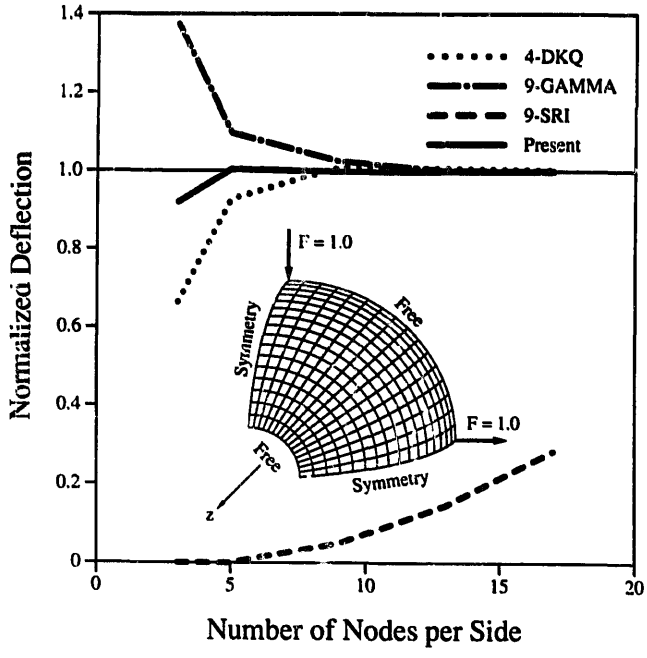

Fig. 7. Description and results of the pinched hemisphere with an 18° hole. Symmetry is used and only one quadrant is modeled. Present results are for the mixed formulation.

Table 13
Normalized results of the full pinched hemisphere

Nodes per side	Present formulations		Other formulations		
	MIXED	DISP	4-SRI	4-RSDS	4-DKQ
5	65.1	46.8	41.2	96.5	75.3
9	96.8	93.3	92.7	97.1	98.5
17	99.3	98.8	98.4	98.9	99.8

7.5.2. *Full hemispherical shell*

The mesh used for this problem is highly skewed for coarse meshes, and leads to less elements for the same number of nodes per side than the previous mesh; for example, a 2×2 mesh produces four elements in (7.5.1) but only three elements in the present situation.

The results of this problem are listed in Table 13 and Fig. 8. An analytical answer of 0.0924 is used to normalize the displacement at the points of application of the forces.

The performance of the proposed element matches that of some of the best bilinear elements reported in the literature.

7.6. *Scordellis–Lo barrel vault*

The Scordellis–Lo barrel vault, a short cylindrical section loaded by gravity forces, is a membrane-dominated problem, which serves to test the ability of the element to model complex states of membrane stresses. The length of the cylinder is $L = 50$, the radius is $R = 25$, the thickness is $t = 0.25$, and the span angle of the section is $\varphi = 80°$. The material

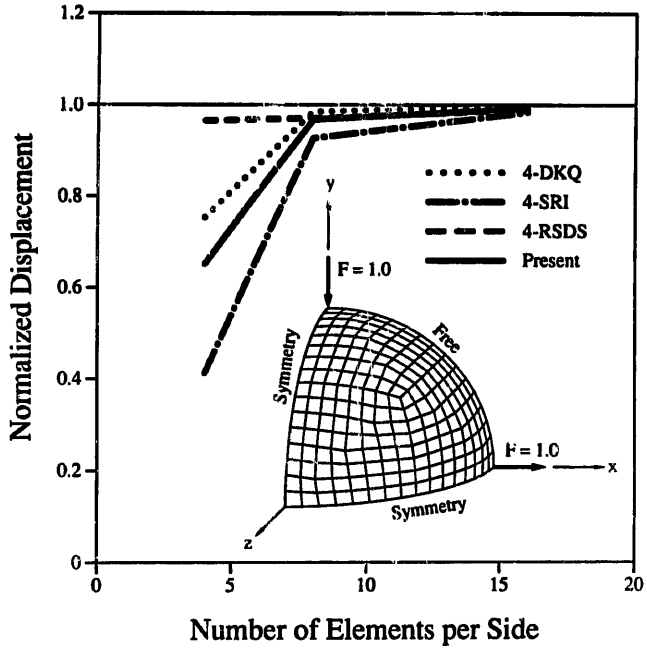

Fig. 8. Description and results of the full pinched hemisphere. Symmetry is used and only one quadrant is modeled. Present results are for the mixed formulation.

Table 14
Normalized results of the Scordellis–Lo barrel vault

Nodes per side	Present formulations		Other formulations		
	MIXED	DISP	4-SRI	4-RSDS	4-DKQ
3	145.0	119.8	126.3	190.4	139.1
5	108.3	94.4	96.4	120.1	104.8
9	101.5	97.3	98.4	104.6	100.5
17	100.0	99.2	99.9	101.0	99.6

properties are $E = 4.32 \times 10^7$ and $\nu = 0$. The solution to this problem is obtained numerically by Scordellis and Lo [31]. These authors report a value of 0.3024. The results are listed in Table 14 and shown in Fig. 9.

Most of the elements considered converge reasonably, and the proposed element converges to 100.0% of the answer with the 16×16 mesh.

7.7. *Pinched cylinder with end diaphragms*

A short cylinder, with two pinching vertical forces at the middle section, and two rigid diaphragms at the end, is modeled using one octant and applying the appropriate symmetry boundary conditions. The length of the cylinder is $L = 600$, the radius is $R = 300$, and the thickness is $t = 3$. The material properties are $E = 3 \times 10^6$ and $\nu = 0.3$.

The numerical results are presented in Table 15 and Fig. 10, normalized against the analytical solution of 1.82488×10^{-5}.

This problem, by far, is the most demanding of all cases considered. It is a severe test of the inextensional bending and complex membrane states of stress. Most four-node shell elements

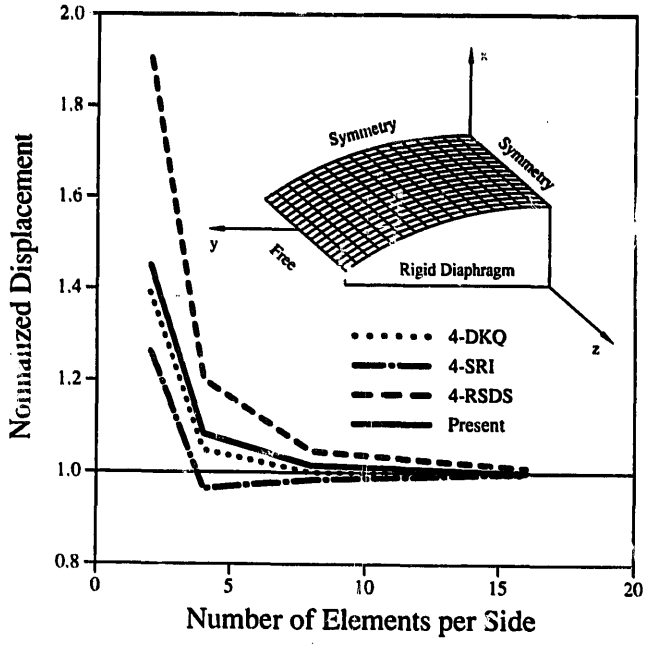

Fig. 9. Description and results of the Scordellis–Lo roof. Symmetry is used and only one quadrature is modeled. Present results are for the mixed formulation.

Table 15
Normalized results of the pinched cylinder

Nodes per side	Present formulations		Other formulations		
	MIXED	DISP	4-SRI	4-RSDS	4-DKQ
5	39.9	37.5	37.3	46.9	63.6
9	76.3	75.6	74.7	79.1	95.1
17	93.5	92.7	93.5	94.6	101.6

do not converge efficiently in this problem, except the discrete Kirchhoff formulations. The present formulation is among the best performers of the bilinear elements which account for shear deformation.

7.8. *Effects of mesh distortion*

To study the effect of mesh distortion on the performance of the proposed element, two problems are examined: a coarse mesh modeling a simply supported plate and a cantilevered beam modeled with one row of elements.

7.8.1. *Simply supported plate*

A simply supported plate under a central point load is modeled with a coarse 2×2 element mesh (Fig. 11). Beginning with a square mesh, the mesh is distorted by moving the middle node along the diagonal of one of the elements (a distance Δ in both the x- and y-directions). The results are compared with the T1 plate bending element [16], and normalized with the

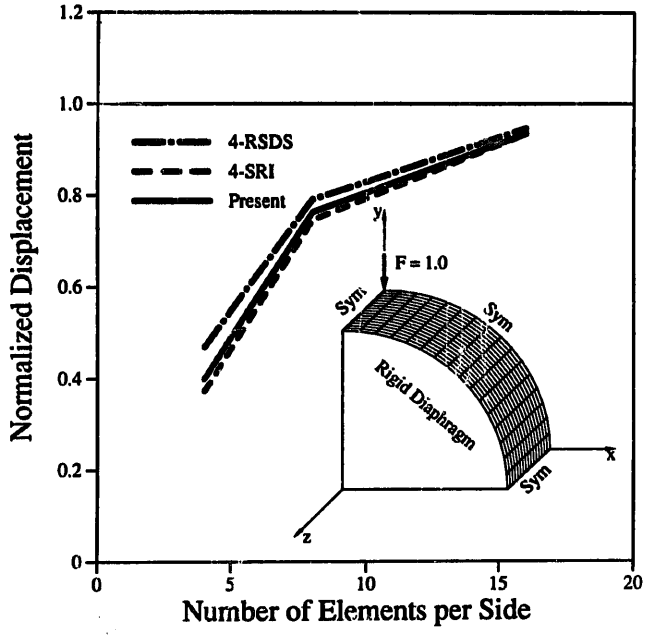

Fig. 10. Description and results of the pinched cylinder with end diaphragms. Symmetry is used and only one eighth of the cylinder is modeled. Present results are for the mixed formulation.

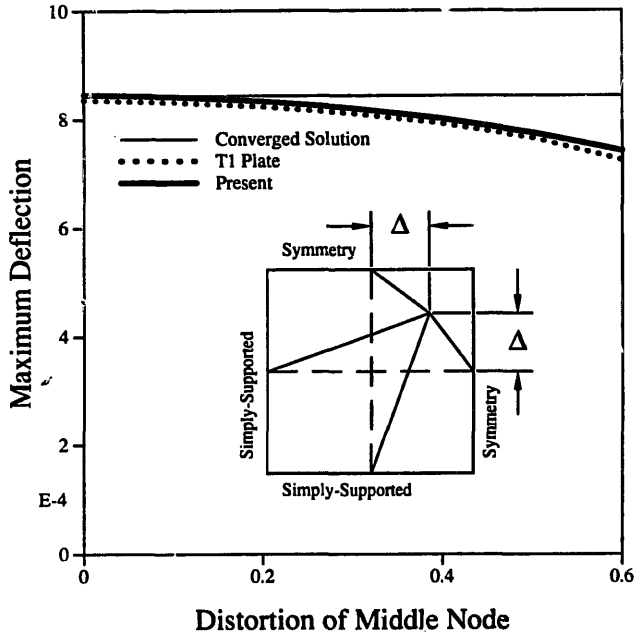

Fig. 11. Effect of mesh distortion on the results of a simply supported plate, subjected to a central bending load. Due to symmetry, only one quadrant is modeled. Present results are for the mixed formulation.

converged finite element solution in Table 16. The performance exhibited by the present element is excellent. Even for the case in which one of the elements exhibits a negative Jacobian (clearly an unacceptable situation), 88% of the value obtained for the undistorted mesh is retained.

7.8.2. *Cantilevered beam*

A cantilevered beam under three different loading conditions, is modeled with a row of ten elements, which are arbitrarily distorted as shown in Fig. 12. The results of the mixed formulation for both meshes are compared to the analytical answers, see Table 17.

Table 16
Results of a simply supported plate

Distance Δ	Present(MIXED)		T1 plate	
	(10^{-4} in)	(%)	(10^{-4} in)	(%)
0.0[a]	8.457	100.2	8.357	99.1
0.1	8.418	99.8	8.316	98.6
0.2	8.333	98.8	8.234	97.6
0.3	8.197	97.2	8.104	96.1
0.4	8.004	94.9	7.918	93.9
0.5[b]	7.746	91.8	7.654	90.7
0.6[c]	7.412	87.9	7.241	85.8

[a]Square mesh.
[b]Jacobian in zero.
[c]Jacobian is negative.

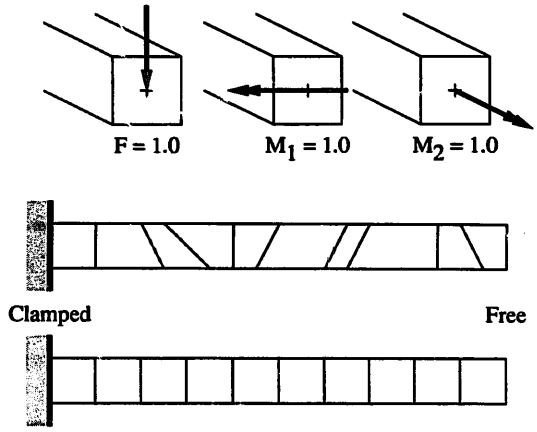

Fig. 12. The distorted and nondistorted meshes and three different loading conditions used on a cantilevered beam to test the proposed element's sensitivity to mesh distortion. Present results are for the mixed formulation.

Table 17
Results of a cantilevered beam

Load type displacement	Bending load		Bending moment		Twisting moment	
	(10^{-3} in)	(%)	(in)	(%)	(10^{-2} rad)	(%)
Square mesh	8.0371	100.5	.012	100.0	2.9578	103.9
Skewed mesh	8.0337	100.4	.012	100.0	2.7559	96.9
Beam theory	8.0000	100.0	.012	100.0	2.8449	100.0

As can be seen from the results, the element exhibits a robust performance highly insensitive to mesh distortion.

8. Concluding remarks

A main thrust of the present work is to demonstrate that shell theories based upon the classical notion of directed media of Cosserat continuum are amenable to an efficient implementation within the framework of the finite element method. We emphasize that the continuum formulation of the shell equations employed here is canonical as is the formulation of the plate equations of the Mindlin–Reissner model. Although one could argue on the form or suitability of a particular constitutive model, the momentum equations in resultant form, and its weak formulation summarized in Table 1, are exact within the realm of the one-director kinematic approximation.

We have shown that the present stress resultant model leads to numerical results in complete agreement with the more cumbersome three-dimensional approach based on the degenerated solid concept. An effort has been made to provide a detailed account of the computational implementation of the model to facilitate and stimulate further comparison and assessment. We have evaluated the proposed finite element formulation through a rather complete set of benchmark problems reported in the literature. Concerning these numerical results, we make the following two observations.

(i) The mixed formulation for the membrane stresses, described in Section 5.1, was initially constructed to alleviate the effects of the so-called *membrane locking* phenomenon. Interestingly enough, our numerical simulations indicate that the full displacement formulation for the membrane and bending fields does not appear to exhibit severe membrane-bending locking problems. Yet, the performance of the mixed formulation is superior to that of the displacement model in all the benchmark cases considered. In particular, a dramatic improvement in the response of the element is obtained with the proposed mixed interpolation for bending stresses in the *singularity-dominated rhombic plate* test. Similar comments apply to the mixed interpolation for the membrane field in membrane dominated problems, such as Cook's membrane test.

(ii) For the pinched cylinder with end diaphragms (Section 7.7), the mixed element considered in this work exhibited similar convergence behavior as the rest of the continuum based formulations tested. By contrast, formulations employing the discrete Kirchoff concept exhibit a clearly superior performance. This behavior seems to indicate that the problem may be related to some form of *shear locking* that is not entirely alleviated by the *assumed strain* method employed. As further numerical evidence in support of this conclusion, we note that if the value of the shear modulus is decreased by a factor of ten, a dramatic improvement in the results is obtained. Since for this thin-shell problem the shear coefficient is, effectively, a penalty parameter that enforces the constraint of zero shear deformation, it would appear that the source of difficulty in this problem should be attributed to the interpolation of shear strains. Nevertheless, our numerical results indicate that the overall performance of the present *stress-resultant based* formulation is comparable, and in some instances superior, to the best performers in the bilinear isoparametric class of *degenerated solid*-based elements.

Acknowledgment

This work was performed under the auspices of the Air Force Office of Scientific Research. Support was provided by grant nos. 2-DJA-544 and 2-DJA-771 with Stanford University. This support is gratefully acknowledged. We wish to thank Professors S. Antman, T. Hughes, P. Krishnaprassad, J. Marsden, C. Steele and R. Taylor for many helpful discussions.

References

[1] D.N. Arnold and R.S. Falk, A uniformly accurate finite element method for the Mindlin–Reissner plate, SIAM J. Numer. Anal. (1988) (to appear).
[2] K.J. Bathe, Finite Element Procedures in Engineering Analysis (Prentice-Hall, Englewood Cliffs, NJ, 1982).
[3] K.J. Bathe and F. Brezzi, On the convergence of a four-node plate bending element based on Mindlin–Reissner plate theory and a mixed interpolation, in: J.R. Whiteman, ed., Proceedings Conference on Mathematics of Finite Elements and Applications V (Academic Press, New York, 1985) 99.491–503.
[4] K.J. Bathe and F. Brezzi, A simplified analysis of two plate bending elements—The MITC4 and MITC9 elements, in: Proceedings Conference NUMETA 87, University College of Swansea, Wales, 1987.
[5] K.J. Bathe and E.N. Dvorkin, A continuum mechanics based four-node shell element for general non-linear analysis, Internat. J. Comput. Aided Engrg. Software 1 (1984).
[6] T. Belytschko, H. Stolarski, W.K. Liu, N. Carpenter and J. S.-J. Ong, Stress projection for membrane and shear locking in shell finite elements, Comput. Meths. Appl. Mech. Engrg. 51 (1985) 221–258.

[7] T. Belytschko and C.S. Tsay, A stabilization procedure for the quadrilateral plate element with one-point quadrature, Internat. J. Numer. Meths. Engrg. 19 (1983) 405–420.
[8] T. Belytschko, J.S.-J. Ong, W.K. Liu and J.M. Kennedy, Hourglass control in linear and nonlinear problems, Comput. Meths. Appl. Mech. Engrg. 43 (1984) 251–276.
[9] F. Brezzi and M. Fortin, Numerical approximation of Mindlin–Reissner plates, Math. Comput. 42 (175) (1985) 151–158.
[10] B. Budiansky and J.L. Sanders Jr, On the "best" first-order linear shell theory, Prog. Appl. Mech. 20 (1963) 129–140.
[11] H.C. Huang and E. Hinton, A nine-node Lagrangian plate element with enhanced shear interpolation, Engrg. Comput. 1 (1984) 369–379.
[12] T.J.R. Hughes, Generalization of selective integgration procedures to anisotropic and nonlinear media, Internat. J. Numer. Meths. Engrg. 15 (9) (1980) 1413–1418.
[13] T.J.R. Hughes, M. Cohen and M. Haroun, Reduced and selective integration techniques in the finite element analysis of plates, Nucl. Engrg. Design 46 (1978) 203–222.
[14] T.J.R. Hughes and W.K. Liu, Nonlinear finite element analysis of shells: Part I. Three-dimensional shells, Comput. Meths. Appl. Mech. Engrg. 26 (1981) 331–362.
[15] T.J.R. Hughes and W.K. Liu, Nonlinear finite element analysis of shells: Part II. Two-dimensional shells, Comput. Meths. Appl. Mech. Engrg. 27 (1981) 167–182.
[16] T.J.R. Hughes and T.E. Tezduyar, Finite elements based upon Mindlin plate theory with particular reference to the four-node bilinear isoparametric element, J. Appl. Mech. (1981) 587–596.
[17] T.J.R. Hughes, The Finite Element Method (Prentice-Hall, Englewood-Cliffs, NJ, 1987).
[18] J.H. Jang and P. Pinsky, A nine-node assumed covariant strain shell element, Internat. J. Numer. Meths. Engrg.
[19] K.K. Liu, E.S. Law, D. Lam and T. Belytschko, Resultant-stress degenerated-shell element, Comput. Meths. Appl. Mech. Engrg. 55 (1986) 259–300.
[20] R.H. MacNeal, A simple quadrilateral shell element, Comput. & Structures 8 (1978) 175–183.
[21] R.H. MacNeal, Derivation of element stiffness matrices by assumed strain distribution, Nucl. Engrg. Design 70 (1982) 3–12.
[22] R.H. MacNeal and R.L. Harder, A proposed standard set of problems to test finite element accuracy, in: Proceedings of AIAA Conference on Structures and Structural Dynamics, Palm Springs, CA, 1984.
[23] L.S.D. Morely, Skew Plates and Structures, International Series of Monographs in Aeronautics and Astronautics (MacMillan, New York, 1963).
[24] L.S.D. Morely and A.J. Morris, Conflict between finite elements and shell theory, Rept., Royal Aircraft Establishment, London, 1978.
[25] P.M. Naghdi, The theory of shells. in C. Truesdell, ed., Handbuch der Physik, Vol Via/2, Mechanics of Solids II (Springer, Berlin, 1972).
[26] F.I. Niordson, Shell theory, North-Holland Series in Applied Mathematics and Mechanics (North-Holland, Amsterdam, 1985).
[27] K.C. Parks and G.M. Stanley, A curved C^0 shell element based on assumed natural-coordinate strains, J. Appl. Mech. 53 (2) (1986) 278–290.
[28] H. Parisch, A critical survey of the 9-node degenerated shell element with special emphasis on thin shell application and reduced integration, Comput. Meths. Appl. Mech. Engrg. 20 (1979) 323–350.
[29] T.H.H. Pian and K. Sumihara, Rational approach for assumed stress finite elements, Internat. J. Numer. Meths. Engrg. 20 (1984) 1685–1695.
[30] J.L. Sanders Jr, An improved first-approximation theory for thin shells, Tech. Rept. R-24, 11, NASA, 1959.
[31] A.C. Scordellis and K.S. Lo, Computer analysis of cylindrical shells, J. Amer. Concr. Inst. 61 (1969) 539–561.
[32] J.C. Simo and D.D. Fox, On a stress resultant geometrically exact shell model. Part I: formulation and optimal parametrization, Comput. Meths. Appl. Mech. Engrg. (1988).
[33] J.C. Simo, J.E. Marsden and P.S. Krishnaprassad, The Hamiltonian structure of elasticity. The convective representation of solids, rods and plates, Arch. Rat. Mech. Anal. (1987) (to appear).
[34] J.C. Simo and L.V. Quoc, A three-dimensional finite strain rod model. Part II: Geometric and computational aspects, Comput. Meths. Appl. Mech. Engrg. 58 (1986) 79–116.
[35] J.C. Simo and L. Vu-Quoc, A beam model including shear and torsional warping distortions based on an exact geometric description of nonlinear deformations, Internat. J. Solids and Structures (1987) (to appear).

[36] J.C. Simo and L. Vu-Quoc, On the dynamics in space of rods undergoing large motions—a geometrically exact approach, Comput. Meths. Appl. Mech. Engrg. (1987) (to appear).
[37] J.C. Simo and T.J.R. Hughes, On the variational foundations of assumed strain methods, J. Appl. Mech. 53 (1) (1986) 51–54.
[38] G. Stanley, Continuum-based shell elements, Ph.D. Dissertation, Applied Mechanics Division, Stanford University, Stanford, CA, 1985.
[39] C.R. Steele, Private Communication, 1987.
[40] H. Stolarski and T. Belytschko, Membrane locking and reduced integration for curved elements, J. Appl. Mech. 49 (1982) 172–176.
[41] H. Stolarski and T. Belytschko, Shear and membrane locking in curved C^0 elements, Comput. Meths. Appl. Mech. Engrg. 41 (1983) 279–296.
[42] R.L. Taylor, Finite element analysis of linear shell problems, in: S.R. Whiteman, ed., Proceedings of the Mathematics of Finite Elements and Applications (MAFELAP 1987).
[43] R.L. Taylor, J.C. Simo, O.C. Zienkiewicz and A.C. Chan, The patch test: A condition for assessing finite element convergence, Internat. J. Numer. Meths. Engrg. 22 (1) (1986) 39–62.
[44] L. Vu-Quoc and J.A. Mora, A class of simple and efficient degenerated shell elements, Rept. No. UCB/SEMM-87/05, Department of Civil Engineering, University of California, 1987.
[45] O.C. Zienkiewicz, The Finite Element Method (McGraw-Hill, New York, 1978).
[46] O.C. Zienkiewicz R.L. Taylor and J.M. Too, Reduced integration technique in general analysis of plates and shells, Internat. J. Numer. Meths. Engrg. 3 (1971) 275–290.